MicroRNA Expression Changes
in Cochlear Nucleus and Inferior Colliculus
after Acute Noise-Induced Hearing Loss

급성 소음성 난청에 의한 와우핵과
하구에서의 마이크로RNA 발현의 변화

2019년 8월

서울대학교 대학원

협동과정 뇌과학 전공

박 소 현

급성 소음성 난청에 의한 와우핵과 하구에서의 마이크로RNA 발현의 변화

지도교수 박 무 균

이 논문을 이학석사 학위논문으로 제출함

2019년 4월

서울대학교 대학원

협동과정 뇌과학 전공

박 소 현

박소현의 이학석사 학위논문을 인준함

2019년 6월

<table>
<tr><td>위 원 장</td><td>이 준 호</td><td>(인)</td></tr>
<tr><td>부위원장</td><td>박 무 균</td><td>(인)</td></tr>
<tr><td>위   원</td><td>석 승 혁</td><td>(인)</td></tr>
</table>

MicroRNA Expression Changes

in Cochlear Nucleus and Inferior Colliculus

after Acute Noise-Induced Hearing Loss

Advisor: Professor Moo Kyun Park, M.D, Ph.D.

A thesis submitted to the Graduate Faculty

of Seoul National University in partial fulfillment

of the requirement for the Degree of Master of Science

Park Sohyeon

Approved by thesis committee

June 2019

Professor	Lee Jun Ho	(인)
Professor	Park Moo Kyun	(인)
Professor	Seok Seung Hyeok	(인)

Abstract

MicroRNA Expression Changes in Cochlear Nucleus and Inferior Colliculus after Acute Noise-Induced Hearing Loss

Sohyeon Park

Interdisciplinary Program in Neuroscience

Seoul National University Graduate School

Noise-induced hearing loss (NIHL) is one of the most common auditory disorders and a major socioeconomic problem. NIHL can lead to secondary changes that induce neural plasticity in the central auditory pathway. These changes include decreases in the number of synapses, degeneration of auditory nerve fibers, and reorganization of the cochlear nucleus (CN) and inferior colliculus (IC). Either prevention of auditory hair cell (HC) death or treatment at an early stage is critical to preserve hearing. MicroRNAs (miRNAs) can silence

.

complementary sequences within mRNA molecules and are important regulators of biological processes such as cell differentiation, proliferation, and survival. This study investigated the role of miRNAs in the neural plasticity of the central auditory pathway after acute NIHL.

Four groups of 6-week-old Sprague–Dawley rats (each group: n = 12; no. of ears = 24) were used in this study. One group was assayed 1 day after noise exposure (1N), another group was assayed 3 days after noise exposure (3N), and the other two groups were the 1-day and 3-day control groups. Anesthetized animals were exposed to 2 h of white-band noise (2–20 kHz) at 115 dB in a sound-proofed chamber. Auditory brainstem response (ABR) thresholds were measured using a Smart EP system. The amplitude of waves II and IV and the latency of waves IV–II were evaluated. Bilateral CN, IC and cochleae were harvested at Day 1 and Day 3 after noise exposure. Paraffin sections of the organ of Corti were stained using hematoxylin and eosin and evaluated for morphological changes. In addition, whole mount surface preparations were stained using phalloidin and HCs were counted. The Affymetrix miRNA 4.0 GeneChip was used for the microarray analysis

of miRNAs from the CN and IC. Candidate miRNAs were validated using quantitative reverse transcription polymerase chain reaction (qRT-PCR), and putative miRNA target pathways were identified.

Normal hearing levels were verified using the ABR thresholds of the 1-day (4 kHz, 20.6 ± 2.2 dB; 8 kHz, 21.3 ± 2.7 dB; 16 kHz, 25.4 ± 3.6 dB) and 3-day (4 kHz, 20.8 ± 2.4 dB; 8 kHz, 21.9 ± 3.2 dB; 16 kHz, 25.6 ± 4.3 dB) control groups. ABR thresholds increased significantly in both the 1N (4 kHz, 81.9 ± 11.6 dB; 8 kHz, 87.1 ± 3.3 dB; 16 kHz, 88.3 ± 2.4 dB) and 3N (4 kHz, 78.8 ± 11.8 dB; 8 kHz, 84.6 ± 2.9 dB; 16 kHz, 86.7 ± 3.8 dB) groups. At 3 days after noise exposure, animals exhibited a significant (p <0.001) decreased ABR threshold at all three frequencies (4 kHz, 42.7 ± 17.1 dB; 8 kHz, 51.9 ± 13.7 dB; 16 kHz, 63.5 ± 12.6 dB) compared to animals exposed to 1 day of noise (4 kHz, 65.6 ± 19.5 dB; 8 kHz, 73.7 ± 10.7 dB; 16 kHz, 79.4 ± 8.5 dB). The latencies of waves IV–II were not differ significantly between 1N and 3N rats. However, wave II was significantly larger in the 3N group than in the 1N group at all frequencies (p <0.001). In addition, at 4 kHz, the amplitude of wave IV was slightly greater in the 3N group than in the 1N group (p <0.001).

The middle and apical turn sections of the organs of Corti were intact, whereas in the basal turn sections, the outer HCs and other non-sensory cells were lost. The 1N and 3N rats had similar numbers of surviving HCs, most of the missing HCs were from the outer parts of the basal turn sections. There were significant differences in the basal and middle turn sections of the organs of Corti between the treatment and control groups. No significant differences were observed in the apical turn sections between the two treatment groups. Using a 1.5-fold change of normalized intensity values (p <0.1) as a criterion, we selected 10 candidate miRNAs from the CN and 13 candidate miRNAs from the IC microarray analysis. After validation by qRT-PCR, five miRNAs were retained from the CN candidates (miR-200b-3p, miR-183-5p, miR-411-3p, miR-20b-5p, and miR-377-3p) and three miRNAs were retained from the IC candidates (miR-92a-1-5p, miR-136-3p, and miR-26b-5p).

These results, confirmed using ABR threshold data, show that even short-term acoustic stimulation can cause hearing loss. Changes in the ABR amplitude of wave II suggested that the CN may be particularly important. The microarray analysis and qRT-PCR results suggest that

miR-200b-3p, miR-183-5p, miR-411-3p, miR-20b-5p, miR-377-3p, miR-92a-1-5p, miR-136-3p, and miR-26b-5p may play key roles in the neuroplasticity of the central auditory pathway. An analysis of the five candidate miRNAs from the CN using the Kyoto Encyclopedia of Genes and Genomes (KEGG) database suggested that these miRNAs may be associated with the mitogen-activated protein kinase (MAPK) signaling pathway, axon guidance, and the neurotrophin signaling pathway. A similar analysis of the three candidate miRNAs from the IC also found a potential association with the MAPK signaling pathway. Further studies with miRNA oligomers are needed to validate these candidate miRNAs. Such miRNAs may be used in the early diagnosis and treatment of neural plasticity of the central auditory pathway after acute NIHL.

Contents

List of Figures

List of Tables

Introduction

The structure of the ear and sound perception

A sound wave is a form of mechanical energy, consisting of alternating compressions and rarefactions that travel through the air. Because the brain cannot perceive this mechanical energy, it must be converted into electrical signals, which are then subject to neural analysis. Therefore, ears have unique structures and functions. Ears consist of three distinctive parts: the external, middle, and inner ear; and each part is important for sound perception. The external ear collects sound waves, and when sound reaches the tympanic membrane, it is amplified by ossicles in the middle ear. Finally, mechanical energy is converted into electrical energy in the inner ear [1].

The inner ear comprises two different organs: the vestibule and the cochlea. The vestibule senses movement and the cochlea senses sound. The cochlea contains two fluids, called the perilymph and endolymph. Vibrations that are amplified by ossicles are transferred to the perilymph in the scala vestibule through the oval window. The sound wave in the perilymph displaces the basilar membrane, which moves

1

stereocilia at the top of the hair cells (HCs) and generates a neural response. This mechanotransduction occurs in the HCs of the organ of Corti [2].
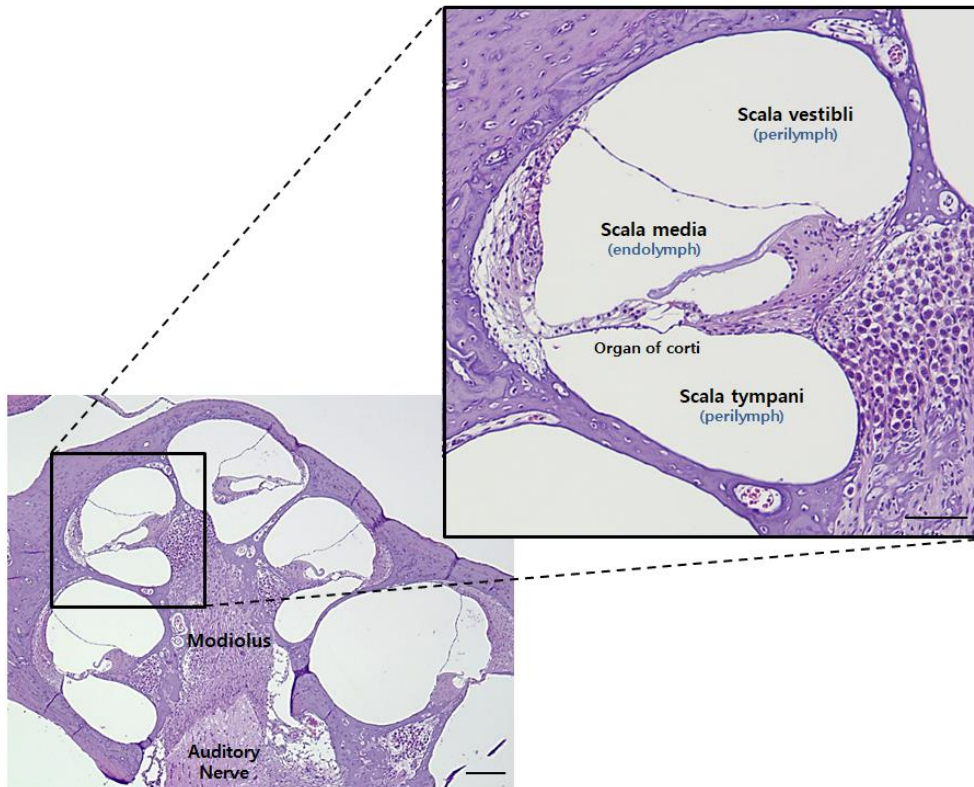

Figure 1. Structure of the cochlea

Hematoxylin and eosin (H&E) staining of a normal rat cochlea. The rat cochlea twists two-and-a-half times and is filled with two types of fluid: perilymph and endolymph [3]. The scale bar on the left represents 200 μm. The scale bar on the right represents 100 μm.

The central auditory pathway

Electrical signals from the HCs flow to primary sensory neurons, which are called spiral ganglion neurons. These cochlear nerves combine with vestibular nerves to become branch VIII of the cranial nerve [1], which transfers the converted acoustic information to the cochlear nucleus (CN), developing the neural pathway [4].

The superior olivary complex (SOC) in the ventral auditory brainstem receives auditory information from the CN and sends the signal to the inferior colliculus (IC). The IC plays a crucial role in the auditory pathway and is the first location where parallel auditory signals from both sides of the cochlea are integrated. Most of the auditory information is processed in the IC and sent to the auditory cortex through the medial geniculate body [5].

Hearing loss

According to the World Health Organization, 466 million people—more than 5% of the world's population—are affected by hearing loss [6].

Hearing plays an important role in daily life. The ability to hear enables people to determine the source of sounds and collect information necessary to function [7]. Hearing is also crucial for communication because it is used to understand and produce speech [1]. Loss of hearing makes communication difficult and can lead to psychosocial problems, such as depression and feelings of loneliness [8]. Therefore, losing the ability to hear can affect people's lives in many ways.

Types of hearing loss

Hearing can be interrupted anywhere along the auditory pathway between the external auditory canal and the auditory cortex, and hearing loss can affect anyone, regardless of age or sex [9]. There are three different types of hearing loss: conductive, sensorineural (SNHL), and mixed hearing loss.

Conductive hearing loss can occur in the outer or middle part of the ear. A structural abnormality, such as a blockage of the ear canal, otitis, or perforation of the tympanic membrane, prevents sound from

reaching the cochlea. SNHL results from damage to the inner ear (e.g., the cochlea), sensory HC loss, or degenerated nerve fibers. In this case, even if sound reaches the cochlea, the brain cannot perceive the signal.

Most forms of conductive hearing loss can be ameliorated using medical or surgical treatments. However, SNHL is generally permanent and the hearing ability cannot be completely restored. SNHL is often treated using hearing aids and cochlear implants [10].

Hearing loss can be categorized according to the location of the impairment, its causes, and severity. In addition to the three types of hearing loss described above, there are other factors that can lead to hearing impairment. For example, there are infants who are born with congenital malformations or have genetic defects that lead to impairment. In addition, some adults develop hearing disorders as a result of occupational or recreational noise, or the use of particular drugs [11].

Noise-induced hearing loss (NIHL)

NIHL is a type of acquired hearing loss that is due to a sudden excessively loud sound or to continuous moderately loud sounds. Depending on the duration and intensity of the sounds, hearing loss can be temporary or permanent [12]. Sounds that are less than 75 dB sound pressure level (SPL) are considered normal and are unlikely to cause hearing loss. However, sounds that are greater than 85 dB SPL can lead to physical damage to the ear [13]. In general, daily conversation is equivalent to 60 dB, the sound of a vacuum cleaner is approximately 85 dB, a hairdryer or a subway train is approximately 100 dB, personal listening devices (PLDs) and chainsaws are approximately 105 dB, and a loud rock concert is approximately 115 dB [14]. The permissible exposure times are 8 h for 85 dB and 2 h 30 min for 90 dB of noise. Because SPL is an ineffective measure of impact on the human ear, A-weighted decibels (dBA) are used to evaluate ear responses. A 2-fold increase in sound intensity is equivalent to a 3-dB increase. For example, 8 h of exposure to 90 dBA is equivalent to 4 h of exposure to 93 dB. Exposure to 115 dBA for a duration of more than 28 s would result in damage to the ear [14, 15].

6

Different factors can cause NIHL, with occupational and recreational noise being the most common among these. People who use PLDs are also increasingly at risk of NIHL [11]. Except in cases of acoustic trauma, NIHL usually progresses slowly over a period of years, making it difficult to recognize. Initial symptoms include difficulty in differentiating conversations against background noise. Later, listening becomes difficult even in ordinary circumstances. Because NIHL progresses gradually and prevention is so crucial, it is important to diagnose NIHL at an early stage [15].

MicroRNAs (miRNAs)

MiRNAs are small non-coding single-stranded endogenous RNAs that regulate posttranscriptional gene expression. Mature miRNAs are 18–22 nucleotides in length and can repress and degrade target mRNAs by binding to their 3′ or 5′ untranslated regions. MiRNAs are involved in a number of physiological processes and play key roles in neural development and plasticity. MiRNAs are abundant in the brain, due to its complexity [16, 17], and are also found in body fluids such as the

cerebrospinal fluid, whole blood, plasma, and serum [18]. Consequently, miRNAs can be detected and analyzed non-surgically and may provide the basis for a new generation of therapeutic agents [19].

Study aims

Noise exposure is one of the most common causes of hearing loss. Exposure to loud noise leads to secondary changes such as decreases in the number of synapses, degeneration of auditory nerve fibers, and reorganization of the CN and IC, which may induce neural plasticity in the central auditory pathway. MiRNAs are important regulators of mRNA molecules. Therefore, this study investigated the role of miRNAs in the neural plasticity of the central auditory pathway after NIHL.
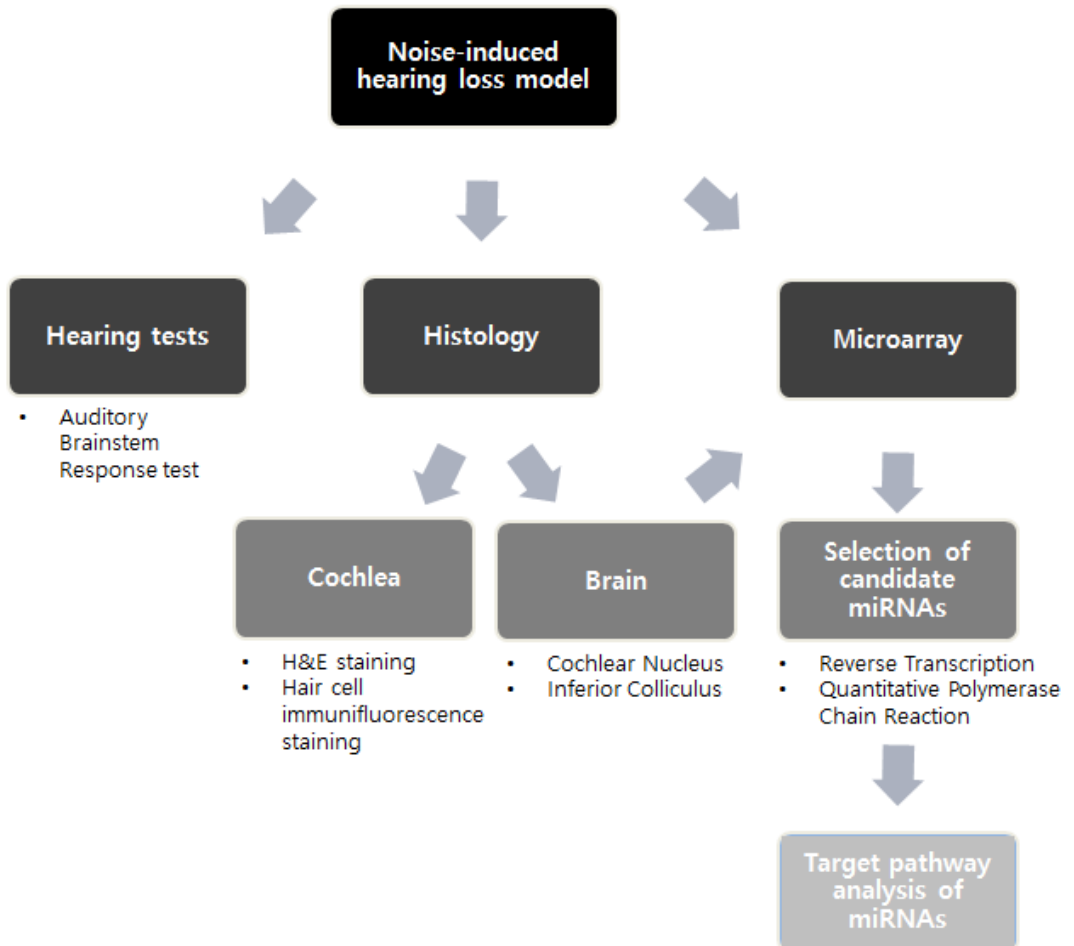
Materials and Methods

Study design

Figure 2. A schematic illustration of the entire experiment

Noise-induced hearing loss (NIHL) was achieved by exposing subjects to 2 h of noise at 115 dB sound pressure level (SPL). Tests of the auditory brainstem response (ABR) and histological examinations of the cochleae confirmed loss of hearing. Microarray analysis of the cochlear nucleus (CN) and inferior colliculus (IC) tissues were used to identify candidate microRNAs (miRNAs). These miRNAs were validated using quantitative reverse transcription polymerase chain reaction (qRT-PCR) and target pathway analysis.

Animal subjects

All of the animal experiments described were approved by the Institutional Animal Care and Use Committee of Seoul National University Hospital (Seoul, Republic of Korea; 18-0025-C1A0), which is endorsed by the Association for the Assessment and Accreditation of Laboratory Animal Care International. The animals used in these experiments were kept under 12-h/12-h day/light cycle conditions with free access to food and water. They were acclimated to laboratory conditions 1 week prior to the initiation of these experiments. A total of 48 male Sprague–Dawley rats, aged 6 weeks, were randomly separated into four groups (all, $n = 12$). One group was assayed 1 day after noise exposure (1N), one group was assayed 3 days after noise exposure (3N), and the other two groups were used as the 1- and 3-day controls.

Noise-Exposure Protocol

Animals were anesthetized using a mixture of 40 mg/kg Zoletil (Zoletil 50; Virbac, Bogotá, Colombia) and 10 mg/kg xylazine (Rumpun; Bayer-Korea, Seoul, Republic of Korea) via intramuscular injection before noise exposure. Each animal was placed in a separate wire cage to avoid unequal noise exposure, and each experiment was performed in a customized acrylic box in a sound-attenuating laboratory booth (900 × 900 × 1,720 mm) with an electromagnetic shield. The animals were exposed to 2 h of broadband white noise at 115 dB SPL using a 2,446-J compression driver (JBL Professional, Los Angeles, CA, USA) with an MA-620 power amplifier (Inkel, Incheon, Republic of Korea) to create the bilateral NIHL animal model. The sound intensity within the acrylic box was measured every hour using a CR152B sound level meter (Cirrus Research plc, Hunmanby, UK) to confirm that there were no alterations in sound level during the noise-exposure treatments. The control animals were injected with the same dose of anesthetic and kept in the sound attenuating booth for the same period of time without noise exposure [20]. Audiometry was performed at 4 h after noise-exposure treatments, to allow stable measurements to be recorded. The experimental procedure is shown in Figure 3.
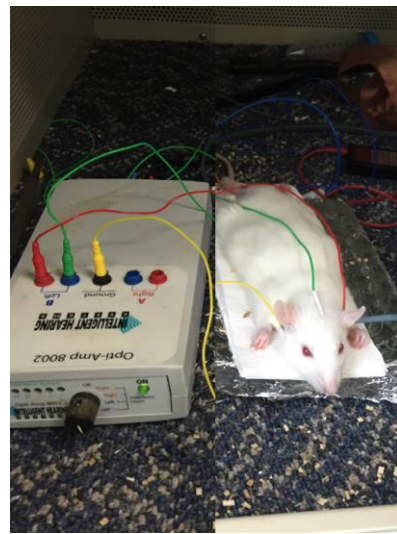
12

A
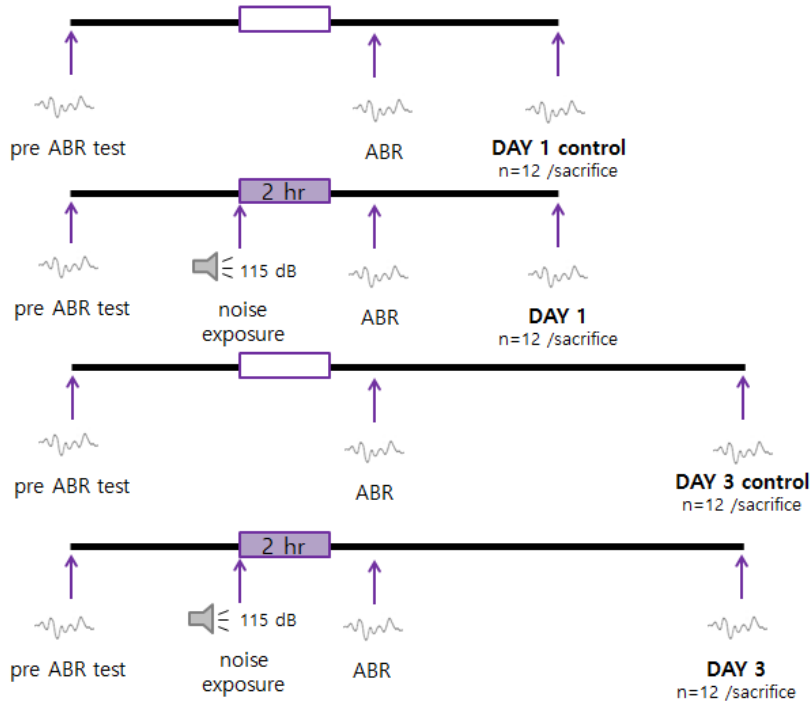
B

C

Figure 3. Noise-exposure protocol

(A) Anesthetized animals were exposed to 2 h of white band noise (2–20 kHz) at 115 dB SPL in a sound-proofed chamber. The empty boxes indicate control conditions. Animals in the control groups were anesthetized and placed in sound-attenuating booths for the same time durations. (B) A photograph of the noise-exposure experiment in progress. A speaker is attached to the top of the acrylic box. (C) Subdermal needle electrodes were positioned at the nape of the neck, the ipsilateral mastoid, and the contralateral mastoid.

Auditory Brainstem Response (ABR) Recordings

The hearing function of all animals was evaluated before noise exposure using the ABR. Animals were anesthetized and placed in sound-attenuating booths. Subdermal needle electrodes were positioned at the nape of the neck as the vertex, the ipsilateral mastoid as the negative, and the contralateral mastoid as the ground [21]. Sound stimuli tone-bursts of 4, 8, and 16 kHz (duration, 1,562 μm; CoS shaping, 21 Hz) were applied. High-frequency software (ver. 3.30; Intelligent Hearing Systems, Miami, FL, USA), and high-frequency transducers (HFT9911-20-0035; Intelligent Hearing Systems) were used to measure the ABR. Before obtaining the electroencephalography signal, the impedance between the electrodes was assessed to establish whether this was less than 2 kΩ. Responses to the signal were amplified approximately 100,000-fold and band-pass filtered (100–1,500 Hz). The intensity of the stimuli ranged from 90 to 20 dB SPL in 5 dB increments. A total of 512 sweeps were averaged at each intensity level. Additional ABR measurements were recorded at 4 h, and on Days 1 and 3 after noise exposure. The ABR threshold was defined as the smallest stimulus intensity level that produced a visible waveform for wave II or IV.

15

Cochlear Whole-Mount Surface Preparation

Both control (n = 8) and noise-exposed (n = 8) animals were sacrificed under anesthesia. For each sample, the cochlea was detached from the temporal bone and fixed in 4% paraformaldehyde solution for 24 h at 4°C. Fixed ears were washed 3 times in 1× phosphate-buffered saline (PBS) [22]. The thin layer of laminar bone covering the cochlea was trimmed under a SZ2-ILST stereomicroscope (Olympus Corporation, Tokyo, Japan) using a drill (Strong 90; Saeshin Precision, Daegu, Republic of Korea) with a 2 mm-diameter diamond burr attachment (Fig. 4A). A hole was created by breaking the bone between the oval and round windows using very fine forceps (Fig. 4B, C). The laminar bone was removed using a conventional 1-mm syringe needle (Fig. 4D–F). The cochlear nerve was cut and the spiral structure of the organ of Corti was isolated. Next, the stria vascularis and Reissner's membrane were removed (Fig. 4G, H). The first turn from the top of the organ of Corti was removed using scissors. This was called the 'apical turn' section. A second turn was removed and called the 'middle turn' section and a final half-turn section was removed and called the 'basal turn' section (Fig. 4I). The sections were placed in 1× PBS solution to prevent them from drying out.
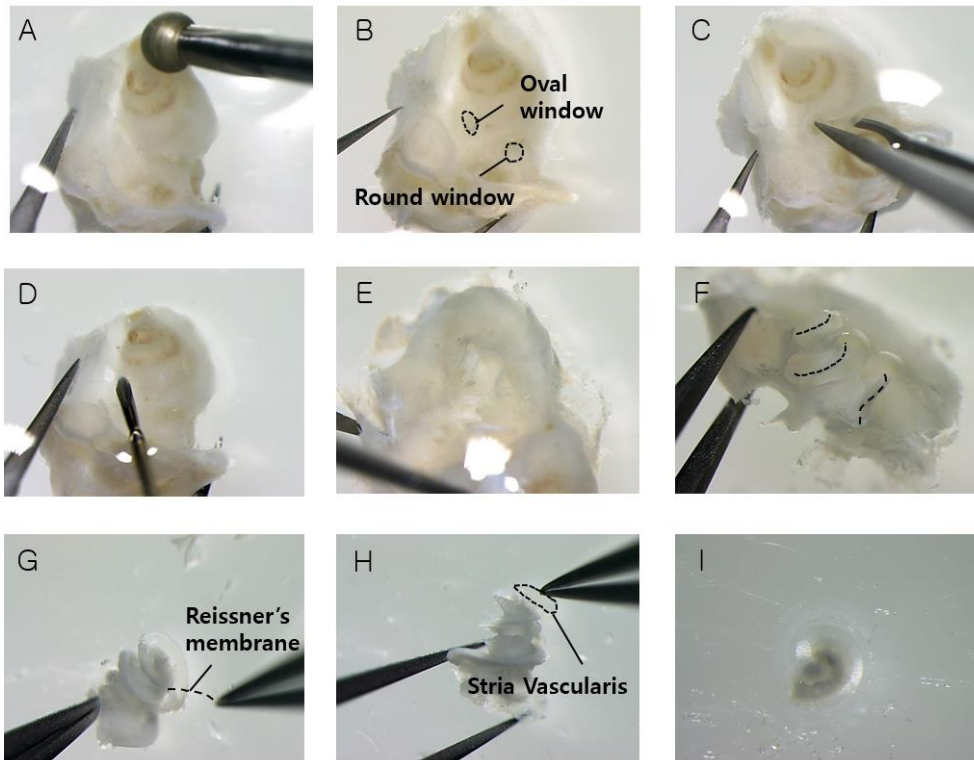
Figure 4. The cochlear whole-mount surface preparation procedure

(A) Drilling the laminar bone that covers the cochlea. (B) and (C) Breaking the bone between the oval and round windows. (D), (E), and (F) Isolating the spiral structure from the organ of Corti. (G) and (H) Removing the Reissner's membrane and stria vascularis. (I) The apical turn section that was removed from the top.

Outer HC staining

Phalloidin was used to stain F-actin, and the photostable orange fluorescent Alexa Fluor 546 dye was used to visualize the cuticular plate and stereocilia within the HCs. After surface preparation, the isolated spiral structure of the organ of Corti was incubated in a mixed solution of 0.3% Triton X-100 and Alexa Fluor 546 phalloidin (1:100 dilution; Invitrogen, Carlsbad, CA, USA) for 45 min at room temperature in a lightproof box [23]. The sample was washed three times in 1× PBS and separated into three segments using Vannas capsulotomy scissors (E-3386; Karl Storz SE & Co. KG, Tuttlingen, Germany): the apical, middle, and basal turn sections. The first complete turn from the apex was the apical turn, the next complete turn was the middle turn, and the final half-turn was the basal turn. Each turn section was mounted on a slide using ProLongTM Gold Antifade mountant (P36930; Invitrogen) to prevent the fluorescent dyes from fading. Images were generated using a STED CW confocal laser scanning system (Leica, Wetzlar, Germany) and HCs within the images were counted.

Cochlear histology

Cochleae from both control (n = 8) and noise-exposed (n = 8) rats were fixed and washed. Samples were decalcified using 10% (w/v) ethylenediaminetetraacetic acid (Santa Cruz Biotechnology, Dallas, TX, USA) in 1× PBS for 4 weeks. A histological examination was performed weekly to determine when the samples were ready for the embedding procedure. The tissues were dehydrated using a series of ethanol washes, and the ethanol was then removed using xylene. After the ethanol was removed, tissues were infiltrated with paraffin wax [24] in a PELORIS II tissue processing system (Leica). The processed cochleae were embedded in a stainless mold and trimmed into 4-μm-thick sagittal sections using a RM2255 microtome (Leica). The sections were deparaffinized for 1 h at 60° C in a dry oven and cleaned using a series of ethanol washes. Next, the nuclei were stained for 7 min with hematoxylin (DAKO, Jena, Germany) and the cytoplasm was stained for 30 s with eosin Y (Sigma-Aldrich, St. Louis, MO, USA). The stained slides were dehydrated and preserved in 70% ethanol [25]. After mounting, the organ of Corti was examined using a light microscope (ECLIPSE Ci-L; Nikon, Tokyo, Japan).

RNA extraction

Whole brain tissue was harvested, and the bilateral CN and IC were dissected out using a brain matrix. The locations of the CN (−9.30 mm to −11.30 mm from the bregma) and the IC (−8.30 mm to −9.30 mm from the bregma) were determined according to the rat brain atlas [26] (Fig. 5). Tissues were frozen in liquid nitrogen immediately after removal and stored at −80°C. The harvested tissue was lysed in 1 mL QIAzol solution using a TissueLyzerII (Qiagen, Hilden, Germany) and incubated at room temperature for 5 min. The samples were placed on a vortex mixer after adding 200 μL chloroform to each and then incubated at room temperature for 3 min. Next, the samples were centrifuged at 12,000 g for 15 min at 4°C and the upper aqueous phase containing the RNA was removed to a fresh tube. A total of 500 μL isopropyl alcohol was added to each tube. The tubes were then inverted and incubated at room temperature for 10 min. Thereafter, the tubes were centrifuged at 7,500 g for 5 min at 4°C and the RNA pellets were washed twice with 1 mL 75% ethanol. The pellets were dried for approximately 5 min and redissolved in RNase-free water.
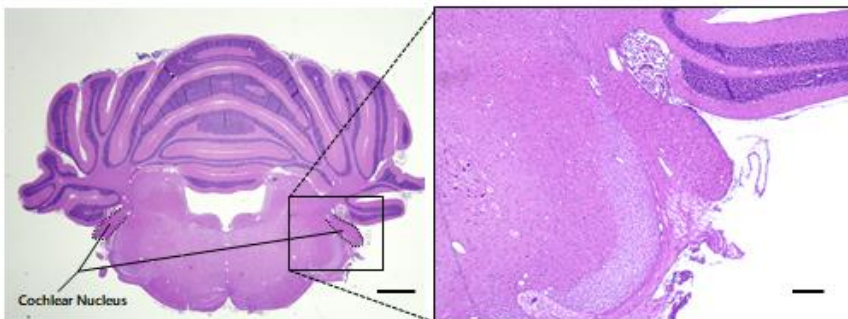
A
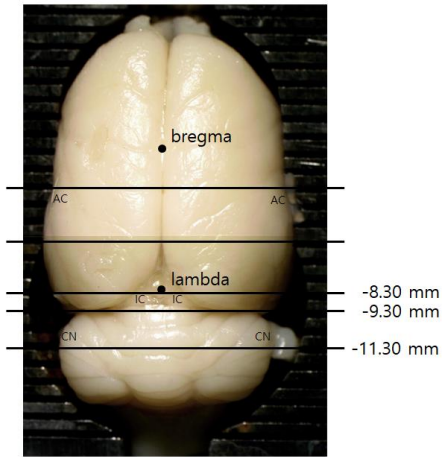
B
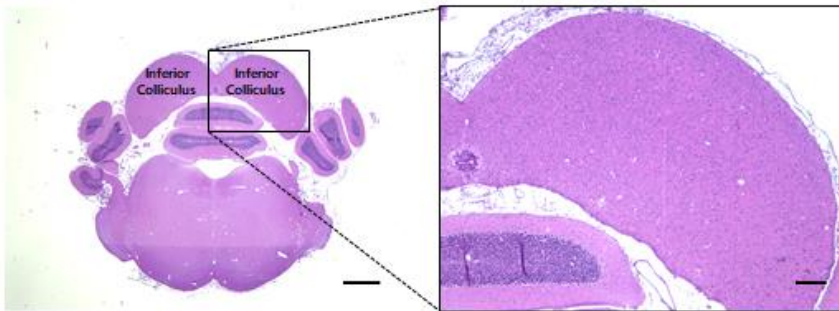
C

Figure 5. Locations of CN and IC.

(A) Slice position for the IC and CN on a stainless brain matrix. (B) Location of the IC based on the rat brain atlas. (C) Location of the CN based on the rat brain atlas.

Analysis of miRNA arrays

The analysis of miRNAs was performed by Ebiogen Inc. (Seoul, Republic of Korea) using the Affymetrix GeneChip miRNA 4.0 array (Affymetrix, Santa Clara, CA, USA). A total of 24 animals were randomly separated into two treatment groups and two corresponding control groups. Treated rats were exposed to noise and assayed after 1 or 3 days. After hearing loss was confirmed, the CN and IC from two animals from the same group were combined and treated as a single sample, and three samples from each group were used for the analysis. Extracted total RNA was assessed for quality and quantity using a Bioanalyzer 2100 system (Agilent, Santa Clara, CA, USA). A total of 250 ng of RNA was analyzed. After ligating biotin-labeled 3DNA dendrimers, each RNA strand was labeled using poly-A polymerase. The biotinylated RNA strands were hybridized for 18 h at 48°C on an Affymetrix GeneChip miRNA 4.0 array. The hybridized GeneChip was washed and stained using an Affymetrix 450 Fluidics station. Fluorescence signals from the 3DNA dendrimers were detected using an Affymetrix GeneChip 3000 7G scanner.

Quantitative reverse transcription polymerase chain reaction (qRT-PCR)

Using an miScript® II RT kit (Qiagen), 2 μg of RNA was mixed with reverse-transcription master mix and incubated for 60 min at 37° C. To inactivate the miScript reverse transcriptase, the mixture was incubated for 5 min at 95° C and then placed on ice. A total of 20 μL of cDNA was diluted to 1:16 and used as template cDNA. The miScript SYBR® Green PCR kit (Qiagen) was used with miScript Primer Assay reagents (Qiagen) for qRT-PCR. U6 small nuclear RNA was used as an endogenous control gene [27]. The miScript Primer Assay reagents and the reaction mix were dispensed into wells containing template cDNA. The PCR plate was sealed with film and centrifuged at 1,000 g for 1 min at room temperature. Initial activation was performed for 15 min at 95° C. The reactions consisted of 40 cycles of denaturation, annealing, and extension, and fluorescence data were collected during the extension phase. The reactions were performed using an ABI 7500 real-time PCR system (Applied Biosystems, Foster City, CA, USA). Relative quantification values were obtained for each of the target genes using the observed cycle threshold (Ct) results and the $2^{-\Delta\Delta Ct}$ method.

Pathway analysis of candidate miRNAs

The CN

For the CN, a total of 10 candidate miRNAs were selected from the microarray analysis based on 1.5-fold changes in normalized intensity values (p <0.1). Of these, five miRNAs were selected following qRT-PCR validation. Using DIANA-miRPath software (ver. 3.0; DIANA TOOLS, www.microrna.gr) a Kyoto Encyclopedia of Genes and Genomes (KEGG) pathway analysis was implemented from DIANA-microT-CDS (ver. 5.0; DIANA-microT-CDS, http://www.microrna.gr/microT-CDS/) with a threshold of 0.8 and a false discovery rate correction [28, 29]. A total of 12 KEGG pathways were identified using a gene union module and a p-value threshold of 0.05.

The IC

For the IC, a total of 13 candidate miRNAs were selected from the microarray analysis based on 1.5-fold changes in normalized intensity values (p <0.1). Of these, three miRNAs were selected following qRT-PCR validation. Using DIANA-miRPath software (ver. 3.0; DIANA TOOLS, www.microrna.gr), a KEGG pathway analysis was implemented from

DIANA-microT-CDS (ver. 5.0; DIANA-microT-CDS, http://www.microrna.gr/microT-CDS/) with a threshold of 0.8 and a false discovery rate correction [28, 29]. A total of 14 KEGG pathways were identified using a gene union module and a p-value threshold of 0.3.

Statistical analyses

All data are expressed as the means ± standard error of the mean, and all data were analyzed using SPSS software (ver. 25; IBM, Armonk, NY, USA). An F-test was performed to determine whether the levels of variation within the groups were equal. After the F-test, data were analyzed using Student's t-tests to identify significant differences between groups. A p-value of <0.05 was considered statistically significant.

Results

Hearing changes after noise exposure

The ABR test measures neural activity in the brainstem and is the most commonly used assessment for animal hearing because it is non-invasive and easy to implement. Tone-burst acoustic stimuli were measured at three different frequencies: 4, 8, and 16 kHz [30]. Our noise-control model (n = 4) showed that the ABR threshold started to decrease at Day 1 after noise exposure. By Day 3 after exposure to noise at 4 and 8 kHz, the ABR thresholds had returned to normal (Fig. 6A).

The mean ABR thresholds observed for the 1-day control group (4 kHz, 20.6 ± 2.2 dB; 8 kHz, 21.3 ± 2.7 dB; 16 kHz, 25.4 ± 3.6 dB), the 1N group (4 kHz, 20.0 ± 0.0 dB; 8 kHz, 20.8 ± 1.9 dB; 16 kHz, 27.1 ± 3.6 dB), the 3-day control group (4 kHz, 20.8 ± 2.4 dB; 8 kHz, 21.9 ± 3.2 dB; 16 kHz, 25.6 ± 4.3 dB), and the 3N group (4 kHz, 24.2 ± 4.8 dB; 8 kHz, 25.8 ± 4.6 dB; 16 kHz, 26.9 ± 3.6 dB) confirmed that hearing levels at all three frequencies were normal before the experiment (Fig. 6B–D).

After 2 h of noise exposure, both the 1N group (4 kHz, 81.9 ± 11.6 dB; 8 kHz, 87.1 ± 3.3 dB; 16 kHz, 88.3 ± 2.4 dB) and the 3N group (4 kHz, 78.8 ± 11.8 dB; 8 kHz, 84.6 ± 2.9 dB; 16 kHz, 86.7 ± 3.8 dB) exhibited significant increases in ABR thresholds compared to the 1-day control group (4 kHz, 20.2 ± 1.0 dB; 8 kHz, 20.4 ± 1.4 dB; 16 kHz, 23.5 ± 3.8 dB) and the 3-day control group (4 kHz, 20.4 ± 1.4 dB; 8 kHz, 21.0 ± 2.5 dB; 16 kHz, 24.4 ± 3.7 dB), respectively (Fig. 6B–D).

At 4 kHz, the mean ABR threshold of the 1N group (65.6 ± 19.5 dB) was slightly lower than that of the 1-day control group (81.9 ± 11.6 dB). Moreover, the mean ABR threshold of the 3N group (42.7 ± 17.1 dB) was lower than that of the 1N group. The differences between these groups were significant ($p < 0.001$; Fig. 6B, E). At 8 kHz, the mean ABR thresholds of both the 1N (73.3 ± 10.7 dB) and 3N (51.9 ± 13.7 dB) groups were significantly lower than that of the control groups (87.1 ± 3.3 dB; $p < 0.001$; Fig. 6C, F). The mean ABR thresholds of the 1N (79.4 ± 8.5 dB) and 3N (63.5 ± 12.6 dB) groups were also significantly lower than that of the control groups (88.3 ± 2.4 dB) at 16 kHz ($p < 0.001$; Fig. 6D, G). The 3N group exhibited significantly better hearing than the 1N group at all three frequencies ($p < 0.001$; Fig. 6E–G).
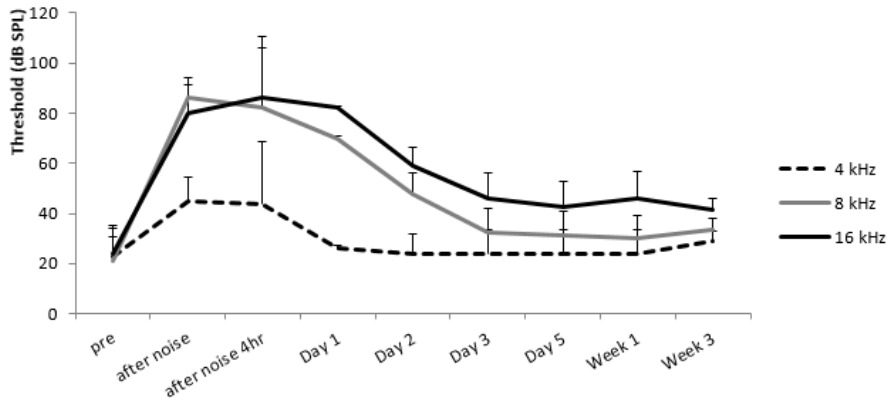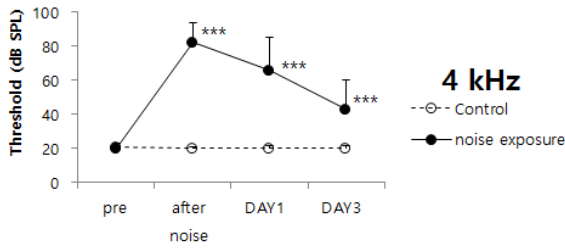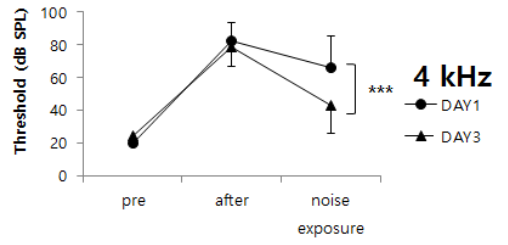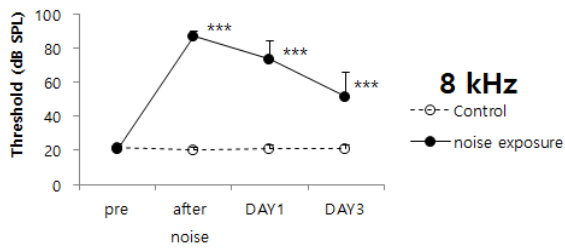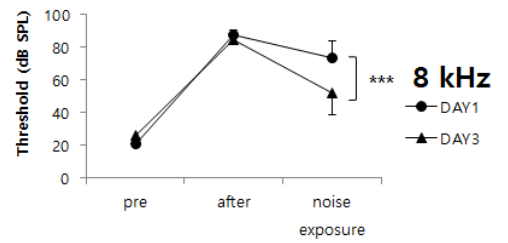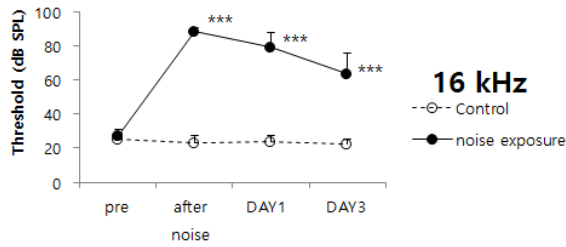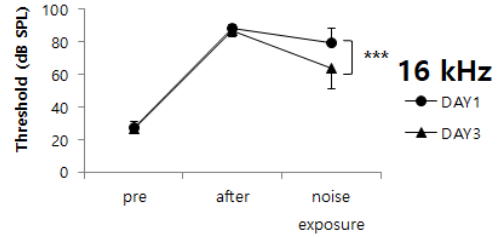
D

G

Figure 6. Hearing changes after noise exposure.

(A) Long-term ABR data for the noise-control model over a period of 3 weeks. (B)–(D) Line graphs showing differences between control groups and treatment groups at frequencies of 4, 8, and 16 kHz. Thresholds for treatment groups were significantly different from those of control groups at all frequencies. Threshold values improved slightly for rats assayed at Day 3 after noise exposure. ***, $p < 0.001$. (E)–(G) Line graphs comparing ABR thresholds in rats assayed at Days 1 and 3 after noise exposure at frequencies of 4, 8, and 16 kHz. ABR thresholds were significantly different between Days 1 and 3 after noise exposure. ***, $p < 0.001$.

ABR latencies

Latencies between waves IV and II were evaluated from the ABR waveforms that were recorded.

At 4 kHz, there was no difference between the latencies observed in the 1N group (2.54 ± 0.50 ms) and the 3N group (2.64 ± 0.77 ms). Similarly, there was no difference between the latencies observed in the 1N group (2.77 ± 0.15 ms) and the 3N group (2.80 ± 0.41 ms) at 16 kHz. Conversely, at 8 kHz, the latency observed in the 3N group (2.38 ± 0.54 ms) was slightly shorter than that observed in the 1N group (2.68 ± 0.71 ms). However, this difference was not significant (Fig. 7A).
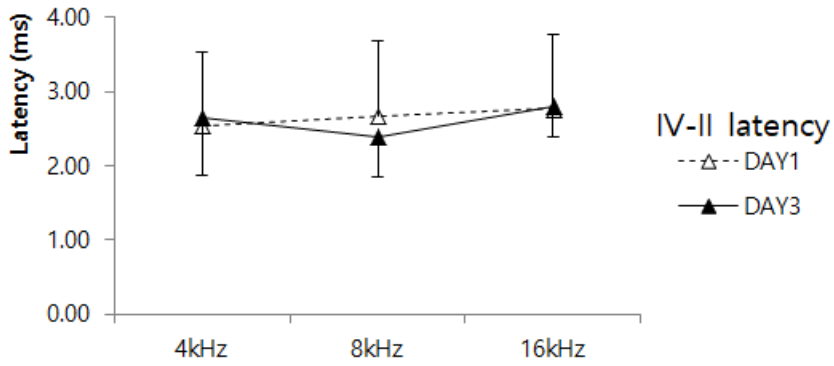
ABR amplitudes

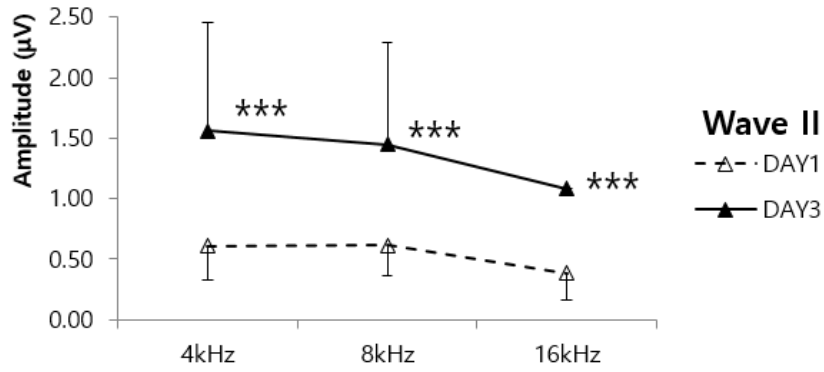The amplitudes of waves II and IV were evaluated from the ABR waveforms that were recorded.

The wave II amplitudes observed in the 1N group (4 kHz, 0.61 ± 0.28 μV; 8 kHz, 0.62 ± 0.25 μV; 16 kHz, 0.39 ± 0.23 μV) were significantly smaller than those observed in the 3N group at each frequency (4 kHz, 1.56 ± 0.90 μV; 8 kHz, 1.45 ± 0.84 μV; 16 kHz, 1.08 ± 0.0 μV; p <0.001; Fig. 7B).

At 4 kHz, the mean wave IV amplitude observed in the 1N group (0.44 ± 0.39 μV) was significantly smaller than that observed in the 3N group (0.93 ± 0.22 μV). However, at the other frequencies, the amplitudes observed in the 1N group (8 kHz, 0.36 ± 0.22 μV; 16 kHz, 0.26 ± 0.18 μV) did not differ significantly from those observed in the 3N group (8 kHz, 0.43 ± 0.40 μV; 16 kHz, 0.26 ± 0.26; Fig. 7C).
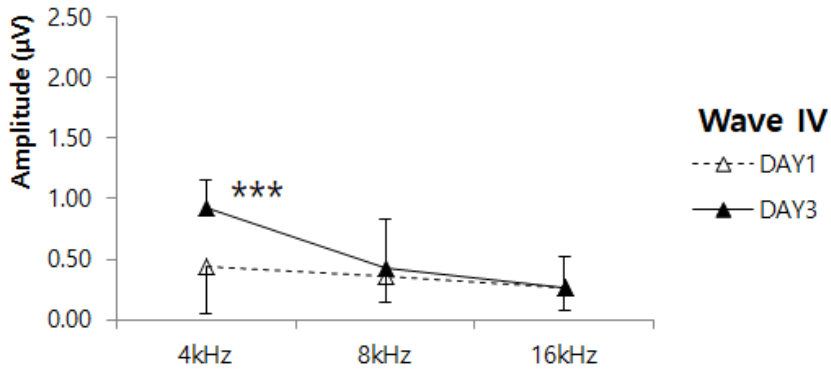
A

B

C

Figure 7. Latencies of waves IV–II and amplitudes of waves II and IV

(A) The latencies of waves IV–II at each frequency. No significant differences were observed at any of the frequencies. (B) A comparison of the amplitude of wave II at different frequencies. The wave II amplitude for rats assayed at Day 3 after noise exposure was significantly larger than that for rats assayed at Day 1 after noise exposure at all frequencies. ***, $p < 0.001$. (C) A comparison of the amplitude of wave IV at different frequencies. The wave IV amplitude for rats assayed at Day 3 after noise exposure was significantly larger than that for rats assayed at Day 1 after noise exposure at 4 kHz. ***, $p < 0.001$. No significant differences were observed at the other frequencies.

Histology of Organ of Corti

A series of sagittal sections from decalcified cochleae were stained with hematoxylin and eosin (H&E) to investigate the structure of the organ of Corti. These structures were intact in the two control groups. The apical turn and middle turn sections of the organs of Corti from the 1N and 3N groups were also normal and contained intact HCs and other non-sensory cells, such as deiter and pillar cells. However, the basal turn sections of the organs of Corti exhibited abnormalities. The degree of damage differed among cochleae. Some exhibited only loss of HCs, whereas others also exhibited loss of supporting cells (Fig. 8).

A

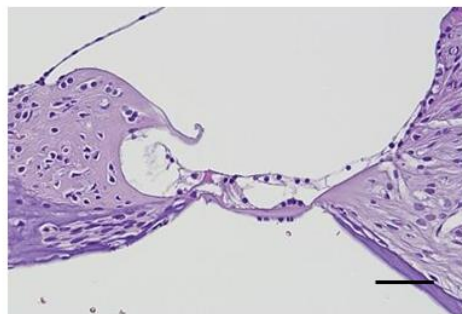|	Basal	Middle	Apical

B

C

36
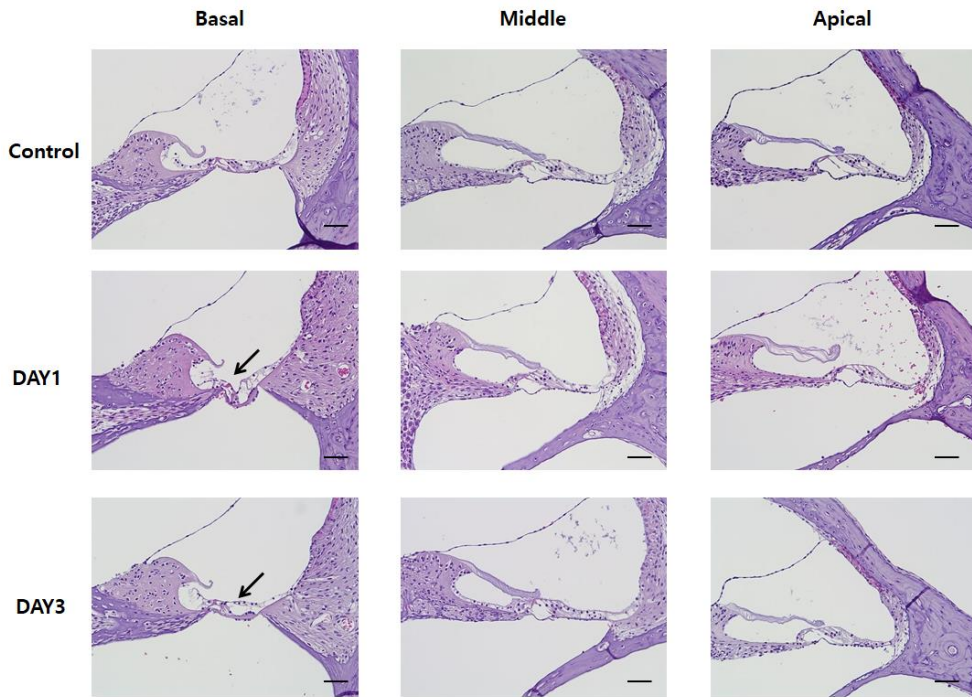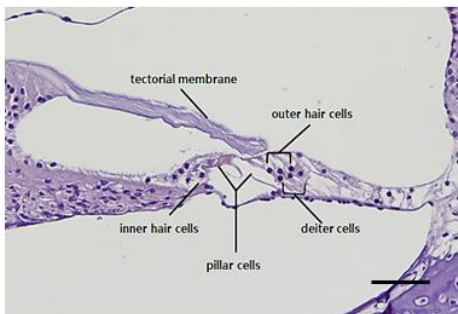
Figure 8. H&E staining of the organ of Corti

(A) Structures of the basal, middle, and apical turn sections of the organ of Corti. Damage (indicated by black arrows) was only observed in the basal turn section in rats assayed at Days 1 and 3 after noise exposure. (B) Examples of intact (left) and damaged (right) organs of Corti. All scale bars represent 50 μm.

Phalloidin Staining of Outer HCs

After the whole mount surface preparation procedure, phalloidin was used to stain the outer HCs. Two 200-μm-long segments were selected from each turn section of the organ of Corti, and the mean numbers of surviving outer HCs were determined.

All three rows of outer HCs from all control samples were normal, and no HCs were missing. However, HCs were lost from the basal turn sections of samples from both the 1N (85% ± 7%; p = 0.001) and 3N (93% ± 6%; p = 0.019) groups. Some HCs were also lost from the middle turn sections of samples from the 1N (99% ± 1%; p = 0.008) and 3N (99% ± 1%; p = 0.000) groups. Outer HCs in the apical turn sections of samples from both the 1N and 3N groups were almost intact (both, 100% ± 0%). For the basal turn sections, significantly fewer HCs were lost from the 3N group than from the 1N group (p = 0.039). No statistically significant differences in HC loss were observed between the 1N and 3N groups for the middle and apical turn sections of the organ of Corti (Fig. 9).

A
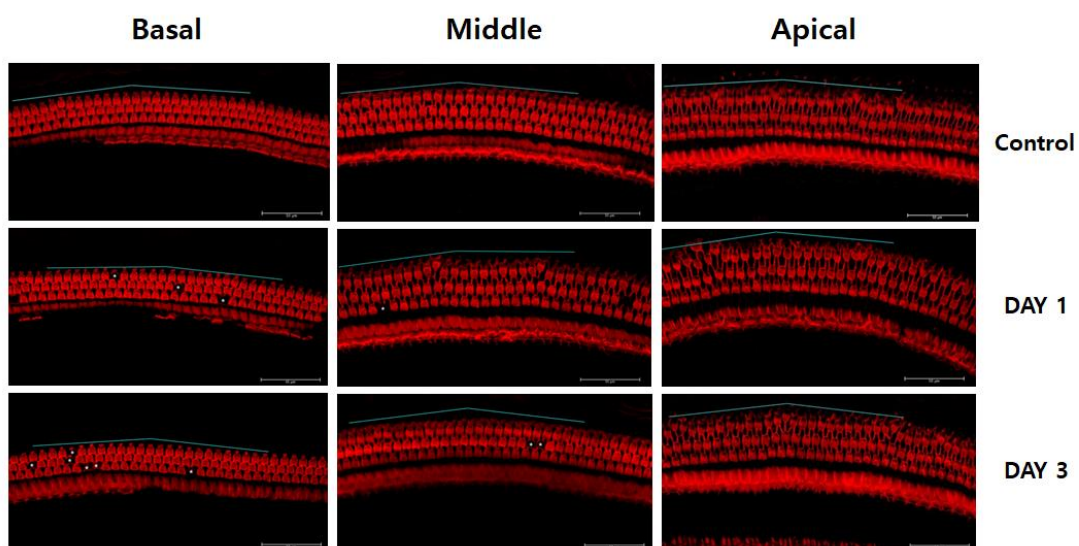
B
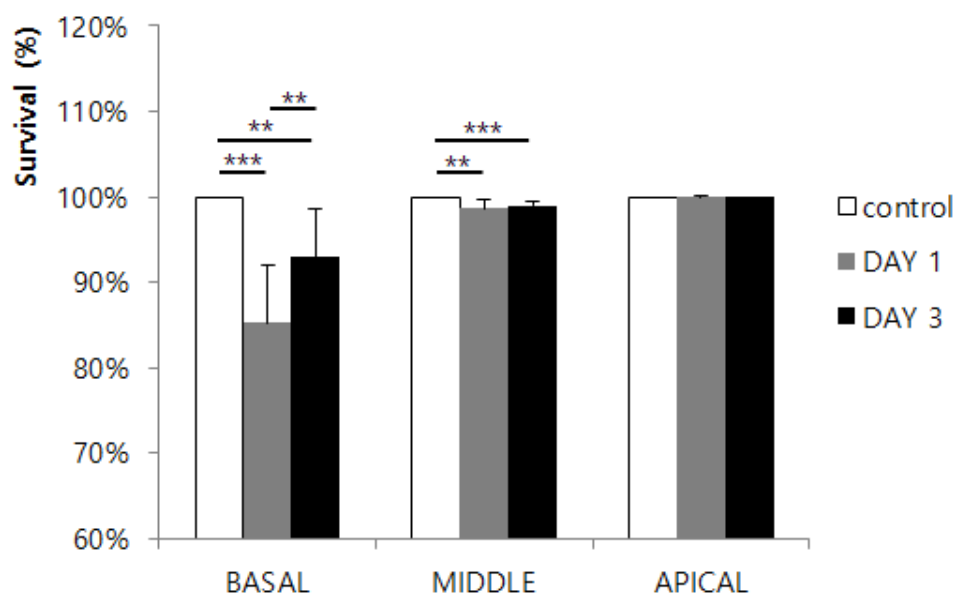
Figure 9. Phalloidin staining of outer hair cells (HCs) and HC survival

(A) Fluorescence staining of outer HCs from each turn section of the cochlea. Scale bars represent 50 μm. Asterisks indicate the positions of lost HCs. (B) Survival rates of outer HCs in each turn section. The number of surviving HCs per 200 μm along the length of the cochlea in the basal, middle, and apical turn sections were counted. **, $p < 0.05$; ***, $p < 0.001$.

Selection of Candidate miRNAs

The CN

The microarray analysis of the CN identified 1,228 miRNAs. Fold changes in expression were assessed across three pair-wise comparisons: between the 1N and 1-day control groups, between the 3N and 3-day control groups, and between the 3N and 1N groups. For each comparison, miRNAs with normalized fold expression change values of more than 1.5 or less than −1.5 (p <0.1) were excluded. Then, the miRNAs from each set were combined and those that overlapped were eliminated. The miRNAs that exhibited expression changes between the 3N and 1N groups and between the 3-day and 1-day control groups were also excluded. A hierarchical clustering heat map was created using Multiple Experiment Viewer (http://mev.tm4.org) to visualize the remaining 33 miRNAs (Fig. 10A). Then, miRNAs with fold expression changes of more than 1.5 or less than 0.5 between the 3-day and 1-day control groups were excluded. Of the 21 miRNAs that remained, only those that are expressed in humans were retained. Therefore, a total of 10 candidate miRNAs were selected: miR-411-3p, miR-183-5p, miR-377-3p, miR-20b-5p, miR-137-5p, miR-211-3p, miR-483-5p, miR-92a-1-5p, miR-187-5p, and miR-200b-3p (Table 1A).

The IC

The microarray analysis of the IC identified 1,200 miRNAs. Fold changes in expression were assessed across three pair-wise comparisons: between the 1N and 1-day control groups, between the 3N and 3-day control groups, and between the 3N and 1N groups. For each comparison, miRNAs with normalized fold expression change values of more than 1.5 or less than −1.5 ($p < 0.1$) were excluded. Then, the miRNAs from each set were combined and those that overlapped were eliminated. The miRNAs that exhibited expression changes between the 3N and 1N groups and between the 3-day and 1-day control groups were also excluded. A hierarchical clustering heat map was created using Multiple Experiment Viewer to visualize the remaining 27 miRNAs (Fig. 10B). Then, miRNAs with fold expression changes of more than 1.5 or less than 0.5 between the 3-day and 1-day control groups were excluded. Of the 26 miRNAs that remained, only those that are expressed in humans were retained. Therefore, a total of 13 candidate miRNAs were selected: miR-204-5p, miR-376b-5p, miR-26b-5p, miR-136-3p, miR-132-5p, miR-128-2-5p, miR-132-3p, miR-377-5p, miR-210-3p, miR-92a-1-5p, miR-425-3p, miR-362-5p, and miR-150-3p (Table 1B).

42
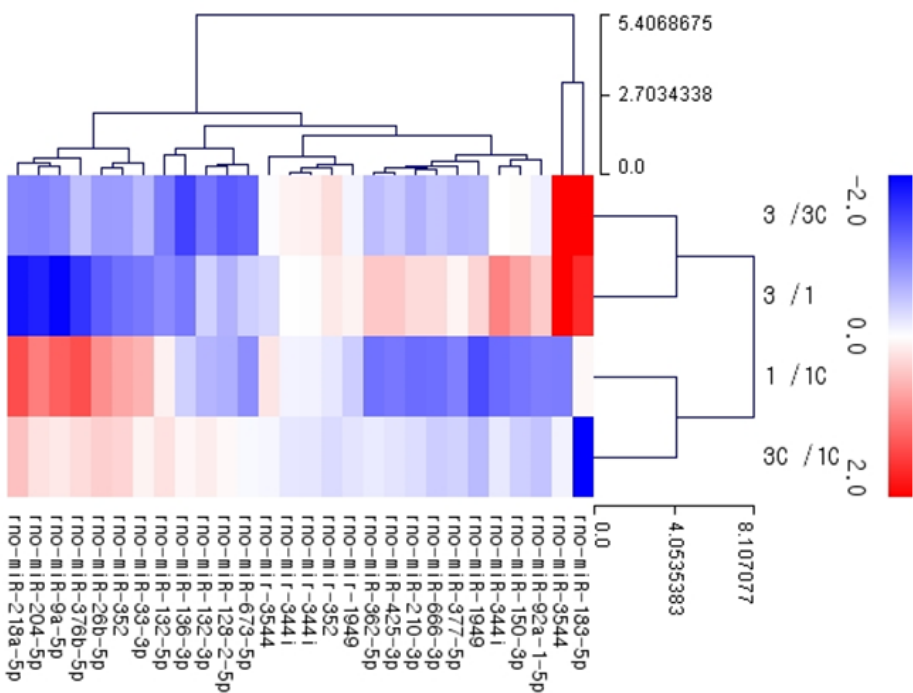
A
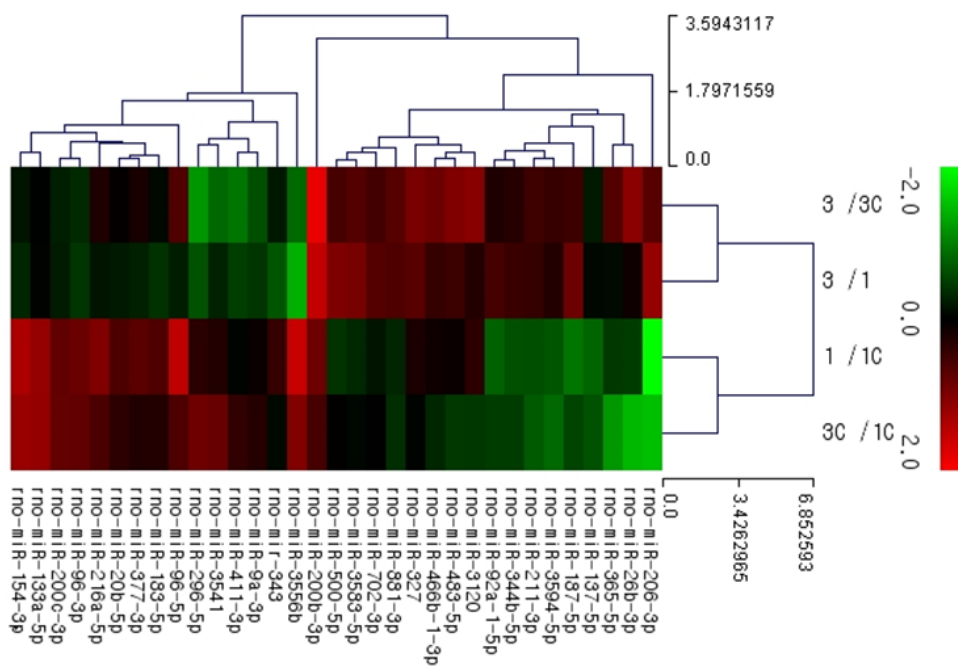
B

Figure 10. Heat maps of the CN and IC.

Heat maps of (A) 33 miRNAs from the CN and (B) 27 miRNAs from the IC selected based on normalized fold change values greater than – 1.5 but less than 1.5 (p <0.1).

A

Gene symbol	Chromosome	Sequence Length	Sequence	1 /1C	3 /3C	3 /1	3C /1C
rno-miR-411-3p	6	20	UAUGUAACACGGUCCACUAA	0.977	0.529	0.712	1.315
rno-miR-183-5p	4	22	UAUGGCACUGGUAGAAUUCACU	1.542	0.957	0.759	1.222
rno-miR-377-3p	6	23	UGAAUCACACAAAGGCAACUUUU	1.652	1.154	0.839	1.201
rno-miR-20b-5p	X	23	CAAAGUGCUCAUAGUGCAGGUAG	1.522	1.029	0.870	1.288
rno-miR-137-5p	2	22	ACGGGUAUUCUUGGGUGGAUAA	0.576	0.871	0.968	0.640
rno-miR-211-3p	1	20	GGCAAGGACAGCAAAGGGGG	0.649	1.420	1.334	0.610
rno-miR-483-5p	1	22	AAGACGGGAGAAGAGAAGGGAG	1.072	2.025	1.393	0.737
rno-miR-92a-1-5p	15	23	AGGUUGGGAUUUGUCGCAAUGCU	0.588	1.194	1.468	0.724
rno-miR-187-5p	18	18	AGGCUACAACACAGGACC	0.529	1.404	1.827	0.688
rno-miR-200b-3p	5	23	UAAUACUGCCUGGUAAUGAUGAC	1.826	3.587	2.895	1.474

B

Gene symbol	Chromosome	Sequence Length	Sequence	1 /1C	3 /3C	3 /1	3C /1C
rno-miR-204-5p	1	22	UUCCCUUUGUCAUCCUAUGCCU	2.020	0.511	0.299	1.181
rno-miR-376b-5p	6	22	GUGGAUAUUCCUUCUAUGGUUA	2.606	0.712	0.332	1.215
rno-miR-26b-5p	9	21	UUCAAGUAAUUCAGGAUAGGU	1.842	0.585	0.413	1.301
rno-miR-136-3p	6	22	CAUCAUCGUCUCAAAUGAGUCU	0.777	0.357	0.484	1.055
rno-miR-132-5p	10	22	ACCGUGGCUUUCGAUUGUUACU	1.085	0.491	0.534	1.180
rno-miR-128-2-5p	8	21	GGGGGCCGAUGCACUGUAAGA	0.650	0.412	0.658	1.039
rno-miR-132-3p	10	22	UAACAGUCUACAGCCAUGGUCG	0.670	0.472	0.782	1.109
rno-miR-377-5p	6	22	AGAGGUUGCCCUUGGUGAAUUC	0.499	0.676	1.066	0.786
rno-miR-210-3p	1	22	CUGUGCGUGUGACAGCGGCUGA	0.452	0.659	1.217	0.834
rno-miR-92a-1-5p	15	23	AGGUUGGGAUUUGUCGCAAUGCU	0.498	0.918	1.333	0.723
rno-miR-425-3p	8	21	AUCGGGAAUAUCGUGUCCGCC	0.479	0.749	1.352	0.865
rno-miR-362-5p	X	24	AAUCCUUGGAACCUAGGUGUGAAU	0.464	0.699	1.353	0.898
rno-miR-150-3p	1	19	CUGGUACAGGCCUGGGGGA	0.474	1.023	1.669	0.774

Table 1. Candidate miRNAs of the (A) cochlear nucleus (CN) and (B) inferior colliculus (IC)

1/1C, comparison between rats assayed 1 day after noise exposure (1N) and 1-day control rats; 3/3C, comparison between rats assayed 3 days

after noise exposure (3N) and 3-day control rats; 3/1, comparison between 3N and 1N rats; 3C/1C, comparison between 3-day and 1-day control rats.

Color index			
Log(2) ratio	Fold	Color	RGB
>3.321928095	>10		150.5.1
>2.9068906	>7.5		200.7.2
>2.321928095	>5		250.8.2
>1.5849625	>3		253.52.47
>1	>2		253.102.98
>0.8073549	>1.75		254.152.148
>0.584962501	>1.5		255.202.201
>0.3219281	>1.25		255.230.229
0	1		255.255.255
<-0.3219281	<0.8		232.229.255
<-0.584962501	<0.6666666		205.205.205
<-0.8073549	<0.5714286		152.162.254
<-1	<0.5		88.104.254
<-1.5849625	<0.3333333		39.59.253
<-2.321928095	<0.2		2.25.244
<-2.9068906	<0.1333333		1.14.137
<-3.321928095	<0.1		1.9.83

Table 2. Color index of fold change for candidate miRNAs.

The color index chart indicates fold changes in expression.

Validation of Candidate miRNAs using qRT-PCR

The CN

Based on the results of the microarray analysis of the CN, the following 10 candidate miRNAs were selected: miR-411-3p, miR-183-5p, miR-377-3p, miR-20b-5p, miR-137-5p, miR-211-3p, miR-483-5p, miR-92a-1-5p, miR-187-5p, and miR-200b-3p (Fig. 11A).

Microarray ratios comparing the 3N and 1N groups and qRT-PCR results are shown in Figure 12A. The following five miRNAs were selected due to their consistent expression patterns: miR-411-3p, miR-183-5p, miR-377-3p, miR-20b-5p, and miR-200b-3p. The expression of miR-200b-3p increased after noise exposure, whereas expression of the other miRNAs decreased after noise exposure.

The IC

Based on the results of the microarray analysis of the IC, the following 13 candidate miRNAs were selected: miR-204-5p, miR-376b-5p, miR-26b-5p, miR-136-3p, miR-132-5p, miR-128-2-5p, miR-132-3p, miR-377-5p, miR-210-3p, miR-92a-1-5p, miR-425-3p, miR-362-5p, and miR-150-3p (Fig. 11B).

Microarray ratios comparing the 3N and 1N groups and qRT-PCR results are shown in Figure 12B. The following three miRNAs were selected due to their consistent expression patterns: miR-92a-1-5p, miR-136-3p, and miR-26b-5p. The expression of miR-92a-1-5p increased after noise exposure, whereas expression of the other miRNAs decreased after noise exposure.

A
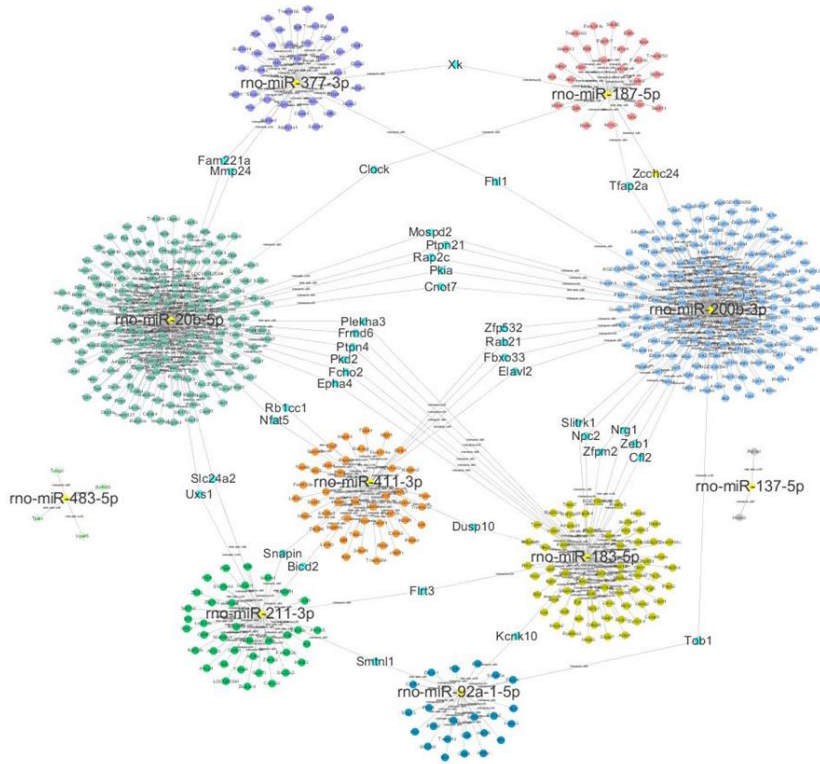
B
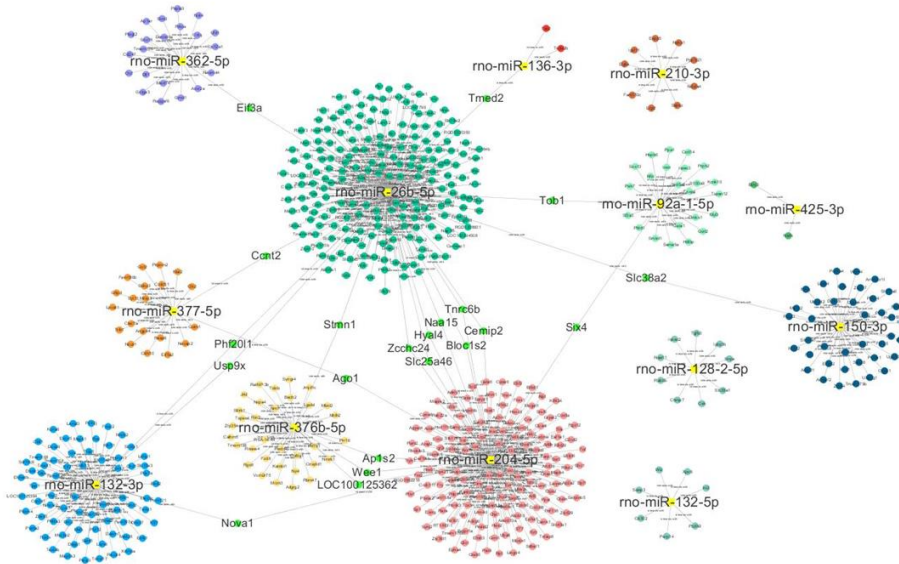
Figure 11. Cytoscape map of the CN and IC

Cytoscape was used to visualize networks among the candidate miRNAs. Only miRNAs that were connected to other miRNAs were selected for validation by qRT-PCR. (A) A total of 10 miRNAs were selected as CN candidate miRNAs: miR-411-3p, miR-183-5p, miR-377-3p, miR-20b-5p, miR-137-5p, miR-211-3p, miR-483-5p, miR-92a-1-5p, miR-187-5p, and miR-200b-3p. (B) A total of 13 miRNAs were selected as IC candidate miRNAs: miR-204-5p, miR-376b-5p, miR-26b-5p, miR-136-3p, miR-132-5p, miR-128-2-5p, miR-132-3p, miR-377-5p, miR-210-3p, miR-92a-1-5p, miR-425-3p, miR-362-5p, and miR-150-3p.

A

B

51
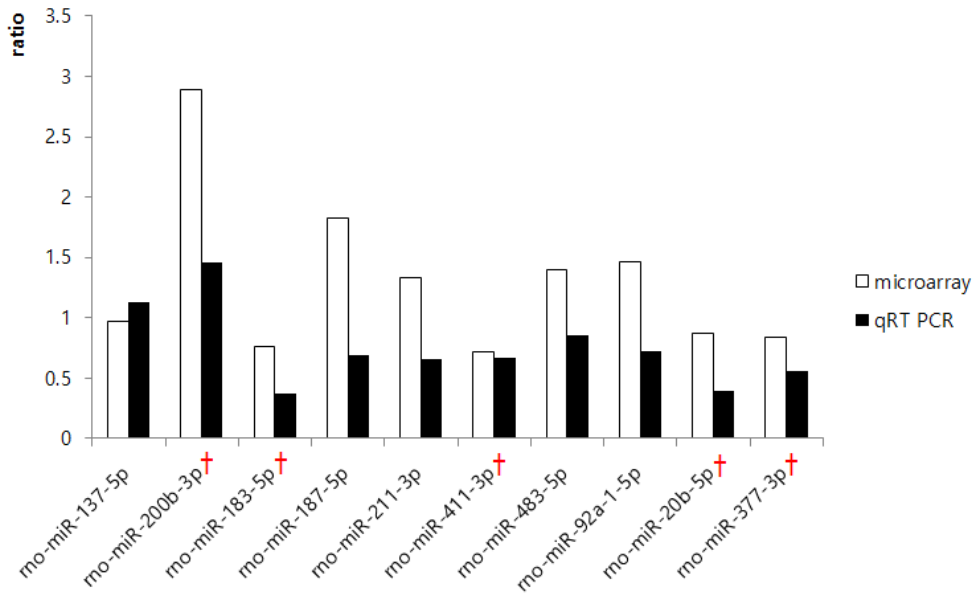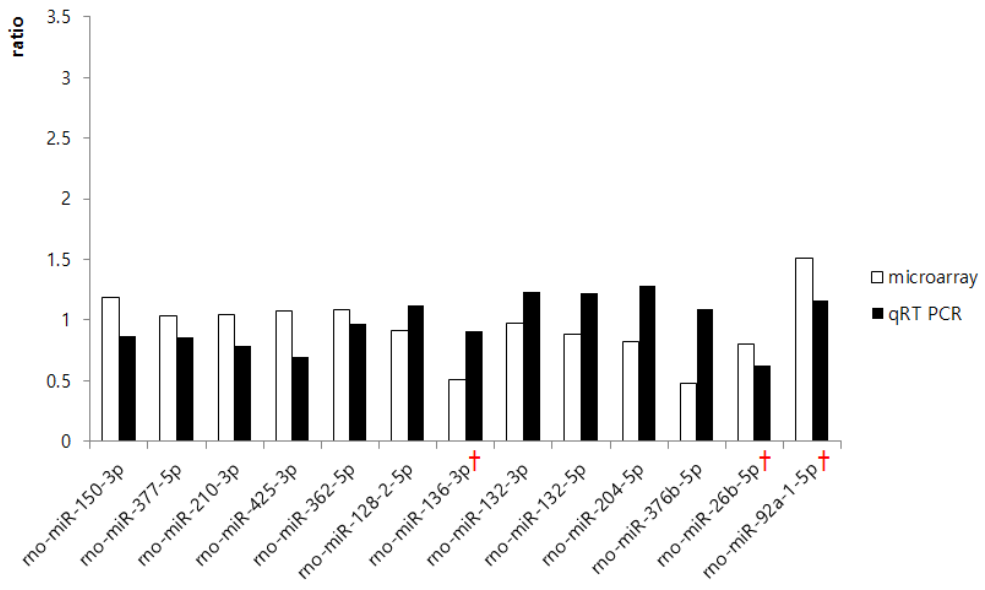
Figure 12. Validation of candidate miRNAs using qRT-PCR

Ratio of expression of each candidate miRNA in the 3N group to expression in the 1N group in the (A) CN and (B) IC. Expression levels were measured using microarray analysis (open bars) and qRT-PCR (filled bars). Crosses indicate validated candidate miRNAs.

Target Pathway Analysis of Candidate miRNAs

The CN

The following five candidate miRNAs expressed in the CN were validated using qRT-PCR: miR-411-3p, miR-183-5p, miR-377-3p, miR-20b-5p, and miR-200b-3p. DIANA-miRPath software (ver. 3.0) was used to investigate the regulation of biological pathways by miRNAs in the CN [28]. A KEGG analysis identified 12 pathways. The most relevant pathways for these miRNAs included those involved in mitogen-activated protein kinase (MAPK) signaling, axon guidance, and transforming growth factor-beta (TGF-β) signaling (Fig. 13A).

The IC

The following three candidate miRNAs expressed in the IC were validated using qRT-PCR: miR-92a-1-5p, miR-136-3p, and miR-26b-5p. DIANA-miRPath software (ver. 3.0) was used to investigate the regulation of biological pathways by miRNAs in the IC [28]. A KEGG analysis identified 14 pathways. The most relevant pathway for these three miRNAs was the MAPK signaling pathway (Fig. 13B).

A
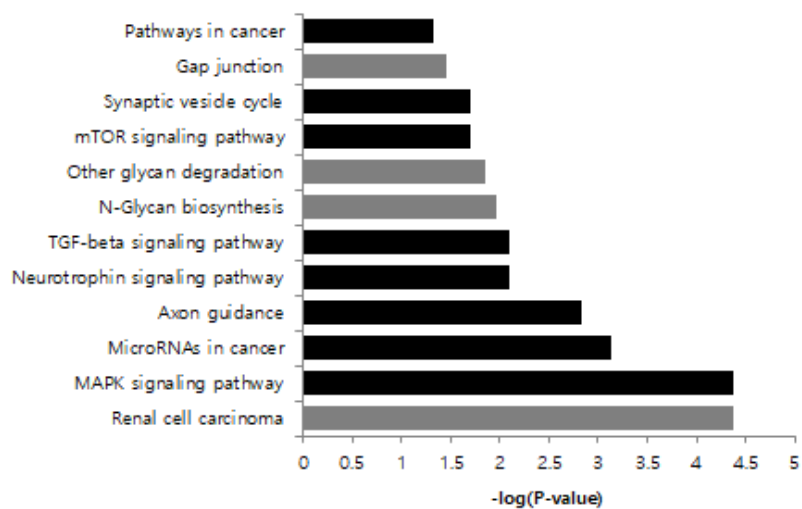
B
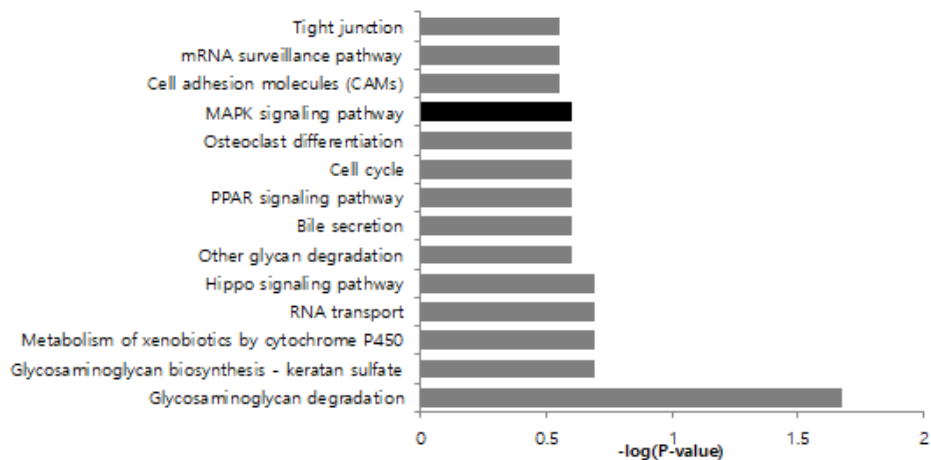
Figure 13. Kyoto Encyclopedia of Genes and Genomes (KEGG) pathway analysis of candidate miRNAs

(A) KEGG pathway analysis for the CN. There were 12 possible *in silico* pathways and the eight pathways marked in black were identified as those most relevant for the five candidate miRNAs. (B) KEGG pathway analysis for the IC. There were 14 possible *in silico* pathways and the mitogen-activated protein kinase (MAPK) signaling pathway, marked in black, was the most relevant for the three candidate miRNAs.

Abbreviations: mTOR, mammalian target of rapamycin; TGF, transforming growth factor; PPAR, peroxisome proliferator-activated receptor.

Discussion

Evaluation of the ABR waves

The ABR test measures neural activity in the brainstem and is the most commonly used assessment because it is non-invasive and easy to implement. The ABR threshold of most animals returns to below 40 dB SPL within 1 week of noise exposure [31]. Consecutive ABR tests were performed in this study and the ABR threshold began to recover on Day 1 after noise exposure. The shift in threshold decreased significantly on Days 2 and 3 after noise exposure and was insignificant after Day 3. Therefore, we hypothesized that significant changes may occur within this time frame, and we used Days 1 and 3 after noise exposure as our two major time points.

Before noise exposure, ABR testing showed that all our animal groups exhibited normal levels of hearing. After noise exposure, the ABR thresholds of the control groups remained normal at all frequencies, whereas the ABR thresholds of the noise-exposure groups increased to more than 70 dB SPL at all frequencies, confirming loss of hearing. The threshold at Day 1 after noise exposure was better than the

threshold at 4 h after noise exposure, and the threshold at Day 3 after noise exposure was better than the threshold at Day 1 after noise exposure. Therefore, the ABR thresholds recovered gradually.

ABR waves consist of five to seven positive vertexes within 10 ms after the sound stimulus. Each positive peak of the wave represents the location of the sound source. The sound signal in the auditory nerve passes through the CN, SOC, lateral lemniscus (LL), IC, and the medial geniculate body and/or the thalamocortical radiations to reach the auditory cortex. In mammals, waves I–V correspond to the auditory nerve, CN, SOC, LL and IC, medial geniculate body, and/or thalamocortical radiations, respectively. However, several studies have shown that the ABR waves of rodents differ from those of other mammals. Waves I, III, and V are used for ABR measurements in humans. Wave II, which corresponds to the CN signal, is the largest wave, and wave III is the smallest wave in rodents [30, 32].

We decided to analyze the CN and the IC because the CN is the origin of central auditory pathway and the IC forms its core. The central auditory pathway receives the bilateral auditory signal [5]. Waves II and IV correspond to the CN and IC. Therefore, we evaluated

the latency between waves IV and II and the height of both these waves from their resting points. The latency between waves IV and II was slightly reduced at 8 kHz in the 3N group, but there were no statistically significant differences in latency at the different frequencies. Changes in the latency of wave I might be expected, because the auditory nerve is the primary region affected after HC loss [33]. An increased latency of wave I may indicate dysfunctional action potential propagation along the auditory nerve [34]. However, it is difficult to measure wave I using the ABR [35]. Moreover, short-term noise exposure may affect auditory nerve fibers but not the CN or IC.

We observed a statistically significant difference in the amplitude of wave II between the 1N and 3N groups. The amplitude of wave II was greater in the 3N group at all frequencies. In general, the ABR amplitude of wave I is reduced by overexpressed sound stimuli [36, 37]. However, the amplitudes of later ABR waves (i.e., II–V) should increase due to compensatory hyperactivity of the central auditory pathway. Reduced sensory input from both ears triggers an increase in excitatory activity and/or a decrease in inhibitory activity [38]. To interpret the ABR wave, latency represents the speed of transmission, whereas

58

amplitude represents the number of neurons that fire together [39]. One possible explanation for these observations is that the number of neurons in the CN has decreased. However, either the damaged neurons have recovered or axonal sprouting from the original neurons must have occurred, because the amplitudes measured were large. Moreover, with the exception of the 4-kHz frequency measurements, there was no difference in the amplitude of wave IV between the two noise-exposure groups. This suggests that the levels of noise used in this study were insufficient to affect the IC, or that neuronal activity in the CN was able to compensate for the damage.

Morphology of the organ of Corti

The cochlea is a spiral-shaped cavity filled with fluid and it consists of three compartments: the scala vestibuli, scala media, scala tympani. The scala vestibuli and scala media are separated by a layer called the Reissner's membrane and the scala media and scala tympani are separated by the basilar membrane. The basilar membrane is a stiff structure on which the organ of Corti is situated. The organ of Corti is

the core structure of the cochlea and it receives sound information. When the amplified mechanical sound information passes through the oval window by the footplate of the stapes, the wave in the perilymph of the scala vestibuli displaces the basilar membrane, which causes movement of HCs. Displacement of the stereocilia at the top of the HCs generates an action potential and the auditory signal is converted to a neural signal. The organ of Corti contains different types of specialized cells and these are responsible for the high degree of sensitivity and selectivity of hearing [40]. There are two types of sensory cells in the organ of Corti—the outer and inner HCs. There are also deiter cells and pillar cells, which have supportive roles.

HC damage or death elevates the hearing threshold, and this is reflected in ABR measurement results. H&E staining was performed to determine whether the organs of Corti in our subjects were intact. We observed abnormalities in one apical turn, two middle turn, and two basal turn sections. Only the region of the organ of Corti close to the oval window exhibited abnormalities. The sections exhibited different patterns of damage. Some slides had only one or two HCs missing, whereas others showed extensive damage together with the loss of

deiter cells and pillar cells, which help to maintain the structure of the organ of Corti. This result indicates that acute acoustic trauma probably affects the basal turn area, which is responsible for high-frequency perception.

Survival of outer HCs

The cochlear HCs are easily damaged by strong sound stimuli and many HCs can die within hours of exposure to noise [41]. Outer HCs amplify the incoming stimulus and are important for hearing sensitivity [42]. The elevation of the hearing threshold after noise exposure can be caused by damage to outer HC electromotility. Therefore, we stained the outer HCs and assessed their capacity for survival.

All three rows of outer HCs in the control groups were normal and there were no missing HCs. Only a few HCs were missing in both the middle and basal turn sections in the 1N and 3N groups. The minimum survival rates of outer HCs in the basal turn and apical turn sections were 78% and 99%, respectively. This suggests that outer HC loss was mild in general. The confirmation of outer HC loss indicates that our

noise-exposure protocol can cause a permanent threshold shift and also implies that only 2 h of noise exposure can permanently damage the cochlea [43].

When a temporary threshold shift (TTS) occurs, the ABR threshold returns to its normal level, although there may be considerable damage to synapses even in the absence of HC loss. Disruption of signaling between the inner HCs and type-1 afferent auditory nerve fibers causes degeneration of the auditory nerve fibers and spiral ganglia. In particular, if synapses connecting low-spontaneous-rate auditory nerve fibers deteriorate, then signal-coding deficits can interrupt communication against background noise [44]. Moreover, a study using a TTS mouse model showed an increase in the rate of age-related hearing loss. [12] Therefore, it is important to protect hearing from noise, regardless of its intensity and duration.

Loss of HCs after noise exposure can lead to secondary damage, including auditory synaptopathy. Noise exposure not only damages the cochlea but also triggers extensive changes in the central auditory pathway. Sensory deprivation due to a decrease in the number of HCs can induce a reduction in cell density in the upper auditory structures.

For example, after overstimulation, the cell population in the ventral CN (VCN) decreases due to apoptosis [45].

Target pathway analysis of candidate miRNAs

It is important to understand the molecular events that occur after acoustic trauma to minimize damage to the central auditory pathway. A bioinformatics analysis by Alagramam *et al.* showed that both 116 and 110 dB of noise exposure could induce genes related to the MAPK signaling pathway [45]. For example, the *Fos* gene, which has a putative role in neuronal apoptosis and cell death, was induced in response to both treatments [46].

Acoustic overstimulation, unlike ablation, can lead to axons dying or degenerating. A study of cats with acoustic trauma demonstrated that new axons can grow in the VCN. Following noise exposure, cochlear nerve endings in the VCN degenerated over a period of several months and disappeared completely after 3 years. However, other small axons subsequently began to appear throughout the VCN, suggesting that degenerated neurons can reorganize the structure of the CN by

generating new axons [47].

The CN is the primary point of convergence between auditory and somatosensory input. The balance of auditory sensory input can be disrupted by a decrease in auditory input from peripheral hearing loss. This imbalance, caused by increased excitatory activity and/or decreased inhibitory activity, enhances central neural receptivity and leads to hyperexcitability [37, 48]. This change in the plasticity of the CN occurs via a form of axonal sprouting, which is regulated by the TGF-β signaling pathway [49]. However, this axonal sprouting can trigger tinnitus, which may cause considerable psychological problems [50]. Therefore, many researchers are trying to find treatments that prevent axonal sprouting by inhibiting the TGF-β signaling pathway.

Among various potential target genes, dual specificity protein phosphatase 10 (*DUSP 10*, Gene ID, 11221) is co-regulated by miR-411-3p and miR-183-5p. The expression of both miR-411-3p and miR-183-5p decreased after acoustic trauma and this increases the levels of DUSP 10. The by-products of DUSP 10 inactivate p38 and stress-activated protein kinase/c-Jun NH(2)-terminal kinase (SAPK/JNK), which inhibits the JNK pathway. In general, the JNK pathway stimulates

apoptosis; therefore, inhibition of the JNK pathway protects cells from apoptosis [51].

Profilin2 (PFN2) is also co-regulated by miR-411-3p and miR-183-5p. The expression of both miR-411-3p and miR-183-5p decreased after acoustic trauma and this increases the levels of PFN2. PFN2 is an actin binding protein that is important for the structure of synapses in neural tissue [52]. In the case of a TTS, afferent synapses are damaged and an increase in PFN2 expression may promote structural recovery of the damaged synapses [53].

Prevention and treatment of NIHL

In most circumstances, SNHL is irreversible because the damaged HCs and neurons do not regenerate. Because there is no curative treatment, preventing NIHL is crucial [14, 54]. Providing information regarding the severity of NIHL and safe levels of noise intensity (i.e., <75 dB) is very important [13]. Using protective devices such as earplugs and earmuffs can also reduce noise trauma. Furthermore, occupational noise-exposure levels must be regulated. Although occupational noise exposure is

65

inevitable in some professions, legislation to regulate exposure limits is required and efforts must be made to reduce noise exposure [14].

There are some promising pharmacological treatments on the horizon. Steroids may have anti-inflammatory effects when provided before or after traumatic noise exposure. For example, pretreatment with dexamethasone was able to preserve retrocochlear auditory neurons [55]. Oxidative stress is also known to damage HCs. Reactive oxygen species have been detected in cochlear tissue immediately after acoustic stimulation. These free radicals can react with various cellular components and affect numerous intracellular processes. N-acetylcysteine is one antioxidant that has been extensively studied and can diminish ototoxic effects. Antioxidants are also associated with fewer adverse effects than steroids. Other antioxidants which could have NIHL protective effects include ginseng, co-enzyme Q10, and vitamins A, C, and E [51, 56].

For some patients with severe hearing impairment, hearing aids and cochlear implants are the best clinical options. Despite advances in technology, it remains impossible for patients to fully recover normal hearing levels [57].

Conclusions

Our results demonstrate that even short-term acoustic stimulation can cause miRNA expression changes in the CN and IC, and these changes may also induce plasticity in the central auditory pathway. Microarray analysis and qRT-PCR validation suggest that miRNAs play a key role in neural plasticity after noise exposure in both the CN (i.e., miR-411-3p, miR-183-5p, miR-377-3p, miR-20b-5p, and miR-200b-3p) and the IC (i.e., miR-92a-1-5p, miR-136-3p, and miR-26b-5p). The candidate miRNAs identified in this study may be involved in regulating the MAPK signaling pathway, axon guidance, and the TGF-β signaling pathway. Numerous studies have investigated NIHL without describing a reliable tool for early diagnosis or a treatment that results in complete recovery. Currently, hearing aids and cochlear implants are used to treat patients with severe hearing loss, but more effective ways to diagnose and treat NIHL are required. Since miRNAs are stable and can be detected in the blood as well as in the brain tissue, these could be targeted in blood tests to help diagnose NIHL earlier. Moreover, gene therapy involving the transfer of miRNAs to target cells using viral vectors or siRNAs may be used to treat NIHL in the future.

References

1.   Kandel, E.R., *Principles of neural science*. 5th ed. 2013, New York: McGraw-Hill. l, 1709 p.

2.   Ekdale, E.G., *Form and function of the mammalian inner ear.* Journal of Anatomy, 2016. **228**(2): p. 324-337.

3.   Albuquerque, A.A., et al., *Understanding the anatomy of ears from guinea pigs and rats and its use in basic otologic research.* Braz J Otorhinolaryngol, 2009. **75**(1): p. 43-9.

4.   Sonntag, M., et al., *Perineuronal nets in the auditory system.* Hear Res, 2015. **329**: p. 21-32.

5.   Ono, M. and T. Ito, *Functional organization of the mammalian auditory midbrain.* J Physiol Sci, 2015. **65**(6): p. 499-506.

6.   World Health Organization. *Deafness and hearing loss*. 2019, March 20; Available from: https://www.who.int/news-room/fact-sheets/detail/deafness-and-hearing-loss.

7.   Yost, W.A., A.N. Popper, and R.R. Fay, *Auditory perception of sound sources*. Springer handbook of auditory research. 2008, New York: Springer. xiii, 331 p.

8.   Barker, A.B., P. Leighton, and M.A. Ferguson, *Coping together with hearing loss: a qualitative meta-synthesis of the psychosocial experiences of people with hearing loss and their communication partners.* Int J Audiol, 2017. **56**(5): p. 297-305.

9.   Lasak, J.M., et al., *Hearing Loss: Diagnosis and Management.* Primary Care, 2014. **41**(1): p. 19-+.

10.   Lee, J.W. and M.L. Bance, *Hearing loss.* Pract Neurol, 2019. **19**(1): p. 28-35.

11.   Eggermont, J.J., *Hearing Loss: Causes, Prevention, and Treatment*. 2017: Elsevier Science.

12.   Le, T.N., et al., *Current insights in noise-induced hearing loss: a literature review of the underlying mechanism, pathophysiology, asymmetry, and*

management options. J Otolaryngol Head Neck Surg, 2017. **46**(1): p. 41.

13. Levihaiem, A., *Noise Induced Hearing Loss: The Impact of Acoustic Trauma on the Ear.* The Science Journal of the Lander College of Arts and Sciences, 2015. **9**.

14. Organization., W.H. *Hearing loss due to recreational exposure to loud sounds: a review.* World Health Organization. 2015; Available from: http://www.who.int/iris/handle/10665/154589.

15. Shin, S.-O., *Updates in Noise Induced Hearing Loss.* Korean Journal of Otorhinolaryngology-Head and Neck Surgery, 2014. **57(9)**(584-588).

16. Tang, C., et al., *The MicroRNA Expression Profiles of Human Temporal Lobe Epilepsy in HS ILAE Type 1.* Cell Mol Neurobiol, 2019. **39**(3): p. 461-470.

17. Minones-Moyano, E., et al., *MicroRNA profiling of Parkinson's disease brains identifies early downregulation of miR-34b/c which modulate mitochondrial function.* Hum Mol Genet, 2011. **20**(15): p. 3067-78.

18. Maffioletti, E., et al., *Peripheral whole blood microRNA alterations in major depression and bipolar disorder.* J Affect Disord, 2016. **200**: p. 250-8.

19. Rupaimoole, R. and F.J. Slack, *MicroRNA therapeutics: towards a new era for the management of cancer and other diseases.* Nat Rev Drug Discov, 2017. **16**(3): p. 203-222.

20. Shi, Z.T., et al., *G-CSF attenuates noise-induced hearing loss.* Neurosci Lett, 2014. **562**: p. 102-6.

21. Chang, M.Y., et al., *The Protective Effect of Egb 761 Against 3-Nitropropionic Acid-Induced Hearing Loss: The Role of Sirtuin 1.* Clin Exp Otorhinolaryngol, 2018. **11**(1): p. 9-16.

22. Paciello, F., et al., *Pioglitazone Represents an Effective Therapeutic Target in Preventing Oxidative/Inflammatory Cochlear Damage Induced by Noise Exposure.* Front Pharmacol, 2018. **9**: p. 1103.

23. Frimmer, M., *What We Have Learned from Phalloidin.* Toxicology Letters, 1987. **35**(2-3): p. 169-182.

24. Zhu, G.J., et al., *Myosin light-chain kinase is necessary for membrane homeostasis in cochlear inner hair cells.* PLoS One, 2012. **7**(4): p. e34894.

25. Fischer, A.H., et al., *Hematoxylin and eosin staining of tissue and cell sections.* CSH Protoc, 2008. **2008**: p. pdb prot4986.

26. Paxinos, G. and C. Watson, *The Rat Brain in Stereotaxic Coordinates.* 2009: Elsevier/Academic.

27. Luo, M., et al., *Selection of reference genes for miRNA qRT-PCR under abiotic stress in grapevine.* Sci Rep, 2018. **8**(1): p. 4444.

28. Vlachos, I.S., et al., *DIANA-miRPath v3.0: deciphering microRNA function with experimental support.* Nucleic Acids Res, 2015. **43**(W1): p. W460-6.

29. Paraskevopoulou, M.D., et al., *DIANA-microT web server v5.0: service integration into miRNA functional analysis workflows.* Nucleic Acids Res, 2013. **41**(Web Server issue): p. W169-73.

30. Alvarado, J.C., et al., *Normal variations in the morphology of auditory brainstem response (ABR) waveforms: a study in Wistar rats.* Neurosci Res, 2012. **73**(4): p. 302-11.

31. Shi, L., et al., *Noise-induced damage to ribbon synapses without permanent threshold shifts in neonatal mice.* Neuroscience, 2015. **304**: p. 368-77.

32. Overbeck, G.W. and M.W. Church, *Effects of tone burst frequency and intensity on the auditory brainstem response (ABR) from albino and pigmented rats.* Hear Res, 1992. **59**(2): p. 129-37.

33. Sugawara, M., G. Corfas, and M.C. Liberman, *Influence of supporting cells on neuronal degeneration after hair cell loss.* J Assoc Res Otolaryngol, 2005. **6**(2): p. 136-47.

34. Tagoe, T., et al., *Auditory nerve perinodal dysmyelination in noise-induced hearing loss.* J Neurosci, 2014. **34**(7): p. 2684-8.

35. Mehraei, G., et al., *Auditory Brainstem Response Latency in Noise as a Marker of Cochlear Synaptopathy.* J Neurosci, 2016. **36**(13): p. 3755-64.

36. Liu, H., et al., *Functional alteration of ribbon synapses in inner hair cells by noise exposure causing hidden hearing loss.* Neurosci Lett, 2019. **707**: p. 134268.

37. Schrode, K.M., et al., *Central Compensation in Auditory Brainstem after Damaging Noise Exposure.* eNeuro, 2018. **5**(4).

38. Shore, S.E., et al., *Dorsal cochlear nucleus responses to somatosensory*

stimulation are enhanced after noise-induced hearing loss. Eur J Neurosci, 2008. **27**(1): p. 155-68.

39. Abadi, S.P., G.M. Khanbabaee, and K.M. Sheibani, *Auditory Brainstem Response Wave Amplitude Characteristics as a Diagnostic Tool in Children with Speech Delay with Unknown Causes.* Iran J Med Sci, 2016. **41**(5): p. 415-21.

40. Ni, G., S.J. Elliott, and J. Baumgart, *Finite-element model of the active organ of Corti.* J R Soc Interface, 2016. **13**(115): p. 20150913.

41. Liberman, M.C. and S.G. Kujawa, *Cochlear synaptopathy in acquired sensorineural hearing loss: Manifestations and mechanisms.* Hear Res, 2017. **349**: p. 138-147.

42. Vinciguerra, P., et al., *Iontophoresis-Assisted Corneal Collagen Cross-Linking with Epithelial Debridement: Preliminary Results.* Biomed Res Int, 2016. **2016**: p. 3720517.

43. Liberman, M.C., *Noise-Induced Hearing Loss: Permanent Versus Temporary Threshold Shifts and the Effects of Hair Cell Versus Neuronal Degeneration.* Adv Exp Med Biol, 2016. **875**: p. 1-7.

44. Shi, L., et al., *Cochlear Synaptopathy and Noise-Induced Hidden Hearing Loss.* Neural Plast, 2016. **2016**: p. 6143164.

45. Basta, D., M. Groschel, and A. Ernst, *[Central and peripheral aspects of noise-induced hearing loss].* HNO, 2018. **66**(5): p. 342-349.

46. Alagramam, K.N., et al., *Noise exposure immediately activates cochlear mitogen-activated protein kinase signaling.* Noise Health, 2014. **16**(73): p. 400-9.

47. Schacht, J. and R.R. Fay, *Auditory Trauma, Protection, and Repair.* 2008: Springer US.

48. Gerken, G.M., *Central tinnitus and lateral inhibition: an auditory brainstem model.* Hear Res, 1996. **97**(1-2): p. 75-83.

49. Mun, S.K., et al., *Losartan Prevents Maladaptive Auditory-Somatosensory Plasticity After Hearing Loss via Transforming Growth Factor-beta Signaling Suppression.* Clin Exp Otorhinolaryngol, 2019. **12**(1): p. 33-39.

50. Bartels, H., M.J. Staal, and F.W. Albers, *Tinnitus and neural plasticity of the brain.* Otol Neurotol, 2007. **28**(2): p. 178-84.

51.   Kurabi, A., et al., *Cellular mechanisms of noise-induced hearing loss.* Hear Res, 2017. **349**: p. 129-137.

52.   Jeong, D.H., et al., *Ubiquitin-proteasome dependent regulation of Profilin2 (Pfn2) by a cellular inhibitor of apoptotic protein 1 (cIAP1).* Biochem Biophys Res Commun, 2018. **506**(3): p. 423-428.

53.   Lobarinas, E., C. Spankovich, and C.G. Le Prell, *Evidence of "hidden hearing loss" following noise exposures that produce robust TTS and ABR wave-I amplitude reductions.* Hear Res, 2017. **349**: p. 155-163.

54.   Imam, L. and S.A. Hannan, *Noise-induced hearing loss: a modern epidemic?* Br J Hosp Med (Lond), 2017. **78**(5): p. 286-290.

55.   Chen, L., et al., *Dexamethasone's effect in the retrocochlear auditory centers of a noise-induced hearing loss mouse model.* Otolaryngol Head Neck Surg, 2014. **151**(4): p. 667-74.

56.   Bielefeld, E.C., et al., *Noise protection with N-acetyl-l-cysteine (NAC) using a variety of noise exposures, NAC doses, and routes of administration.* Acta Otolaryngol, 2007. **127**(9): p. 914-9.

57.   Lee, M.Y., *Gene Therapy for Hearing Protection.* Korean Journal of Otorhinolaryngology-Head and Neck Surgery, 2017. **60(6)**: p. 263-70.

국문 초록

급성 소음성 난청에 의한 와우핵과 하구에서의 MicroRNA 발현의 변화

박소현

협동과정 뇌과학 전공

서울대학교 대학원

현대사회에 있어서 환경스트레스 중 하나인 소음과 개인 청취 기기의 사용이 급증하면서 소음성 난청은 흔하게 발생하는 질병들 중 하나이다. 감각신경성 난청인 소음성 난청은 일차적인 와우의 손상에 이어 이차적으로 시냅스의 감소, 청각신경섬유의 퇴화와 중추 청각 경로의 신경 가소성을 유발할 수 있는 와우핵과 하구의 구조에 영향을 줄 수 도 있다. 그러므로 청력의 보존을 위해서는 유모 세포사의 예방이나 조기치료가 중요하다. MicroRNA (MiRNA)는 특정 mRNA분자내의 상보적 서열을 침묵시킴으로서 세포 분화, 세포 확산 그리고 세포의 생존에 관여하는 생물학적 과정에 중요한 조절 장치이다. 또한 miRNA는 다른

small RNA와는 달리 완벽한 염기 페어링을 필요로 하지 않아서 정확하면서도 좀 더 넓은 범위의 네트워크 조절이 가능하다. 그렇기 때문에 질병의 시작이나 진행에 있어서 miRNA의 관여가 치료법 개발에 큰 도움이 될 수 있다. 이번 실험에서는 일회성의 소음 노출에서 오는 급성 소음성 난청 모델을 만들고, 일시적인 소음이 돌아오는 과정에서 miRNA가 와우핵과 하구에서의 신경가소성 변화에 관여하는 역할을 규명하려고 한다.

총 48마리의 SD 랫드는 1일차 대조군, 소음 노출 후 1일차, 3일차 대조군, 소음 노출 후 3일차 그룹으로 나누어져 실험군은 115 dB SPL에 2시간 동안 노출 되었다. 대조군 또한 같은 시간 동안 마취되어 소음이 없는 조건으로 같은 공간에 놓여 있었다. 청성뇌간반응 검사 (Auditory Brain Stem Response Test, ABR)를 통해 청력의 변화를 확인하고, 각 그룹에서 와우 조직을 채취하여 와우내의 코르티기관을 확인하는 H&E 염색과 유모세포의 생존률을 확인하는 phalloidin 염색을 통해 난청의 유무를 관찰하였다. 또한 중추 청각 경로에서의 시발점인 와우핵, 처음으로 양측 청각 신호의 통합이 일어나는 하구의 microarray analysis와 qRT PCR 검증을 통해 후보 miRNA들을 발견하였고, 그에 따른 추가적인 target pathway analysis와 KEGG analysis를 하였다.

각 실험군들은 대조군들에 비해 청력 역치가 증가하는 것을 보였다.

소음 노출 후 1일차 그룹은 소음 노출 4시간 후 보다 청력 역치가 개선 되는 것을 보였고, 소음 노출 후 3일차 그룹은 소음 노출 1일차 보다 청력 역치가 개선 되는 것을 보였다. 또한 제 2 파형에서 소음 노출 후 3일차 그룹의 진폭이 소음 노출 후 1일차 그룹의 진폭보다 증가하는 것으로 보아 와우핵에서 과잉 민감성 반응이 일어나는 것을 확인 할 수 있었다. 각 그룹에서 코르티 기관을 구조를 관찰 한 결과 실험군은 기저부에서만 손상된 구조를 보였고, 유모세포 형광 면역 염색에서는 기저부와 일부 중간부에서 외유모세포의 손실을 확인하였다. 외유모세포의 손실은 영구적인 청력 손상을 의미하는데, 이로 인해 청각신경섬유 또는 와우핵, 하구에서도 변화가 있음을 예상할 수 있다. 와우핵과 하구를 채취하여 microarray를 실시하였을때, 각 10개와 13개의 후보 miRNA를 선정하였다. 이후 qRT-PCR 검증을 거쳐 와우핵에서는 miR-200b-3p, miR-183-5p, miR-411-3p, miR-20b-5p, 그리고 miR-377-3p 총 5개의 후보군, 하구에서는 miR-136-3p, miR-26b-5p, 그리고, 92a-1-5p 총 3개의 최종 후보군을 선정하였다

제시된 결과들을 통해 단기 음향 자극에 의해서도 충분히 청력 상실을 유발할 수 있음을 확인 할 수 있었다. Microarray analysis를 통해 선별된 miRNA들이 전반적인 중추 청각 경로의 신경가소성의 변화에 중요한 역할을 함을 예상 할 수 있었고, 최종 선정된 miRNA들은 KEGG

analysis를 통해 MAP 인산화 효소 신호 경로, 축삭 인도, 베타 종양 증식 인자 신호 경로 등에 관여함을 예측할 수 있었다. 현재로서는 고도난청환자들을 위한 보청기나 인공와우의 시술이 임상적으로 사용되고 있지만 정상 청력으로의 회복이 불가능하기 때문에 효과적으로 소음성 난청을 진단하고 치료할 수 있는 신개념 치료방법의 개발이 필요하다. MiRNA는 뇌조직 뿐만 아니라 혈액내에서도 매우 안정적으로 발현이 되므로 비외과적인 간단한 채혈을 통해서도 질병의 조기발견의 가능성을 기대할 수 있다. 또한 특정 경로에 관여하는 miRNA를 발견하고 이를 viral vector나 siRNA를 이용하여 대상 세포에 전달하는 식의 유전자 치료를 도입한다면 난청 극복에 유용할 것으로 기대된다.